Centrifugal Magnetophoresis

Author: Daniel Kirby (B.Sc)

Supervisor: Prof. Jens Ducrée

School of Physical Sciences

Dublin City University

Thesis submitted towards a

Doctor of Philosophy

September 2016

Declaration

I hereby certify that this material, which I now submit for assessment on the programme of study leading to the award of doctor of philosophy is entirely my own work, and that I have exercised reasonable care to ensure that the work is original, and does not to the best of my knowledge breach any law of copyright, and has not been taken from the work of others save and to the extent that such work has been cited and acknowledged within the text of my work.

Signed _____

Daniel Kirby, ID: 56390781 Date _____

Acknowledgements

I would like to extend my sincerest thanks and appreciation to the following people for their kind help:
To my Mother and Father, for being the best parents I could ever have hoped for and for supporting me through all of the ups and downs of my time in DCU and to my three brothers, Mike, Damo and Chris, for being a constant support throughout my life.
To my supervisor, Jens, and all the people at the Ducrée group, past and present. You've all been fantastic and it was a pleasure to work with you all.
To everyone at the physics department in DCU, especially Enda, for making my time here so enjoyable. To all at BDI for providing such a great environment to work in and for everything you've ever done to help me along.
To Jonathan Siegrist for starting me off on this journey and to Rob Burger for always knowing everything and being so helpful all the time. To Macdara Glynn for proof reading my thesis and offering excellent advice and humour throughout his time working with me. To Jen, for sharing the stress and strain of frantically finishing a thesis with me.
To three of the physics department's finest, my dear friends Niamh, Tom and Conor who were always there for me and who gave me so much joy, companionship, advice and even a few tears throughout my time here.
To my great friend Brendan Bulfin, for pumping up my ego by always being an inferior scientist. To Kilian, for sharing the great scientific experience of UC Santa Barbara with me, and who now has a permanent share of my heart. To Yaz, Katie and Alan for all the support, sarcasm and gin. To all the old college crew, there's too many of you to mention, but thank you.
To all the lads and ladies back in Westmeath, you've always been great and

you always will be.
To all the Cooleenies and everyone who's lived in or near 22 Cooleen for the unbelievable positivity and creativity you brought to my life.
To Jessie in the DCU health centre and Ruan in the DCU counselling service. You're both amazing people who provide a wonderful service and you helped me so much.
To all the people involved in the drug law reform and abortion rights campaigns for making me feel I could make a difference outside of the lab too. Keep up the amazing work.
To the people who I certainly forgot to include. You're all fabulous.
And finally, to Paulina, who came into my life during the final stages of my PhD, when stress was at its highest and I doubted my research, my motivation and myself. You made me believe that anything was possible and you helped me more than you will ever know. I can't wait to spend the rest of my life with you.

List of publications

Original research articles

1. ***Centrifugo-magnetophoretic particle separation.***
   Daniel Kirby, Jonathan Siegrist, Gregor Kijanka, Laetitia Zavattoni, Orla Sheils, John OLeary, Robert Burger, Jens Ducrée
   Microfluidics Nanofluidics **13** (2012) 899-908

2. ***Rapid and cost-efficient enumeration of rare cancer cells from whole blood by low-loss centrifugo-magnetophoretic purification under stopped-flow conditions.***
   Daniel Kirby, Macdara Glynn, Gregor Kijanka, and Jens Ducrée
   Cytometry Part A **87** (2014) 74-80

3. ***Centrifugo-magnetophoretic purification of CD4+ cells from whole blood toward future HIV/AIDS point-of-care applications.***
   Macdara Glynn, **Daniel Kirby**, Danielle Chung, David J. Kinahan, Gregor Kijanka and Jens Ducrée
   Journal of Laboratory Automation **19** (2013) 285-296

Review articles

4. ***Centrifugal microfluidics for cell analysis.***
   Robert Burger, **Daniel Kirby**, Macdara Glynn, Charles Nwankire, Mary O'Sullivan, Jonathan Siegrist, David Kinahan, Gerson Aguirre, Gregor Kijanka, Robert A Gorkin III, Jens Ducrée
   Current Opinion in Chemical Biology **16** (2012) 409-414

Conference papers

5. ***Immunomagnetic purification of cancer cells from whole blood on a centrifugal microfluidic platform***
   Daniel Kirby, Gregor Kijanka, Jonathan Siegrist, Robert Burger, Orla Sheils, John O'Leary, and Jens Ducrée
   Proceedings of the 16th International Conference on Miniaturized Systems for Chemistry and Life Sciences (μTAS 2012), October 28-November 01, Okinawa, Japan, pages 1126-1128. CBMS, CHEMINAS, 2012

6. ***Reversible immunomagnetic cell trapping and analysis***
   Daniel Kirby, Eanna Bailey, Macrara Glynn, Charles Nwankaire and Jens Ducrée
   Proceedings of the 18th International Conference on Miniaturized Systems for Chemistry and Life Sciences (μTAS 2014), October 26-30, San Antonio, Texas, USA, pages 1292-1294, 2014.

7. ***Continuous, stopped-flow separation for integrated blood cell enrichment and analysis on centrifugal microfluidic platforms***
   Daniel Kirby, Claire O'Connell and Jens Ducrée
   Proceedings of the 4th European Conference on Microfluidics (μFlu2014), December 10-12, Limerick, Ireland, 2014.

8. ***Integration of centrifugo-magnetophoresis and bright-field based T-cell enumeration for HIV diagnostics in resource-poor settings***
   Macdara Glynn, **Daniel Kirby**, Robert Burger and Jens Ducrée
   Proceedings of the 17th International Conference on Miniaturized Systems for Chemistry and Life Sciences (μTAS 2013), October 2731, Freiburg, Germany, pages 964966, 2013.

9. ***Staging the clinical status of cancer patients by chip-based cell enumeration following targetted removal of normal cells from patient blood***
   Macdara Glynn, **Daniel Kirby**, Charles Nwankire, David Kinahan, Cathy Spillane, Orla Shiels, John OLeary and Jens Ducrée
   Proceedings of the 18th International Conference on Miniaturized Systems for Chemistry and Life Sciences (μTAS 2014), October 26-30, San Antonio, Texas, USA, pages 461463, 2014.

10. ***Size and deformability-based particle sorting by strategic design of obstacle arrays in continuous centrifugal sedimentation mode***
    Charles Nwankire, Ivan Maguire, David Kernan, Macdara Glynn, **Daniel Kirby** and Jens Ducrée
    Proceedings of the 18th International Conference on Solid-State Sensors, Actuators & Microsystems (Transducers 2015), June 2125, Anchorage, Alaska, USA, pages 18541856, 2015.

11. ***Isolation of white blood cells using paper triggered dissolvable film valves on a centrifugal platform***
    David Kinahan, Niamh Kilcawley, Macdara Glynn, **Daniel Kirby** and Jens Ducrée
    Proceedings of the 18th International Conference on Miniaturized Systems for Chemistry and Life Sciences (μTAS 2014), October 26-30, San Antonio, Texas, USA, pages 14251427, 2014.

Contributions

- Paper one was originally written by JS and rejected for publication. *DK* was then given first authorship of the manuscript and completely changed and re-wrote the results section with newly designed experiments. *DK* also made significant edits to the materials and methods section and other smaller edits throughout the manuscript. All experimental data and all figures present in the published paper were created solely by *DK*.

- Paper two was entirely written by *DK* and all experimental work and analysis was carried out by him solely. Cell culture work was carried out by MG.

- Paper three was primarily written by MG and was based on work originally undertaken by *DK*. *DK* also designed the experimental apparatus and carried out all calculations.

- Paper four was a review paper primarily written by RB. *DK'S* contributions were Figure 2 and the "cell capturing and assaying" section.

- Paper five was a conference abstract which became the basis of paper three. All work on this abstract was undertaken by *DK* with cell culture work undertaken by GK.

- Paper six was a conference abstract based on *DK'S* own concept and work and entirely written by m*DK*. Experimental assistance was provided by EB and cell culture work was carried out by MG.

- Paper seven was a conference abstract based on *DK'S* own concept and work and entirely written by *DK*. Experimental assistance was provided by COC as well as modifications of figs 6.2-6.4.

- Paper eight was primarily written by MG and based on *DK'S* previous work. *DK'S* contributions were primarily in the first half of the paper. However, *DK* also provided experimental assistance for the rest.

- Paper nine was primarily written by MG with experimental assistance by *DK*. *DK* was also involved in the analysis and use of patient samples and was jointly responsible for decisions on how best to analyse samples in a clinically relevant manner.

- Paper ten was written by CN. Experimental consultation was conducted with *DK*, especially in the area of the technology's possibility to be clinically relevant for circulating tumour cell capture.

- Paper eleven was written by D.Kihanan. *DK* gave experimental advice on blood cell use and its clinical relevance.

Contents

List of Figures

Abstract

Daniel Kirby - Centrifugal Magnetophoresis

Cancer is one of the primary causes of death and long-term illness in the developed world. Early detection before noticeable symptoms appear, or cheap options for population screening and ongoing patient analysis are equally as important as advancements in treatment.

Currently, cancer detection and prognosis happens for the most part *via* a scan or biopsy. If this information could instead be obtained from a simple blood sample the world of cancer treatment and detection would be revolutionised. To that end, this thesis outlines the work undertaken towards completion of a PhD on the topic of magnetophoretic cell handling on a centrifugal microfluidic platform for rare cancer cell detection in blood. This resulted in first using "bio-mimetic" microbeads to prove the physical principle and then using magnetically tagged MCF7 breast cancer cells spiked into a blood sample to simulate circulating tumour cells (CTC's). This strategy proved successful and resulted in detecting magnetically tagged cancer cells in a blood background at a concentration of as low as 1 cell/μl and with a sensitivity of over 80%.

On completion of this phase in the research, the usability of the device using patient blood samples was investigated through a collaboration with pathologists at St. James' Hospital, Dublin. The first step in this phase was to redesign the system to process clinically relevant volumes which, due to the rarity of CTC's in the circulatory system, were on the millilitre scale, as opposed to the microlitre scale. After the redesign it was now possible to successfully analyse 0.2ml of blood and detect cancer cells at a concentration of as low as 0.1 cells/μl.

As well as focusing on the main topic, the author has also investigated various other methods of magnetic and stopped flow particle control for other purposes and all of these also-explored areas of stopped-flow microfluidics fit in well with the broader picture of creating low-cost, easy to use lab-on-a-disc technologies that utilise stopped-flow microfluidic systems and magnetic forces to enable detection of specific cells in blood.

Chapter 1

General Introduction

1.1 Motivation

For a disease which will effect one in three people at some stage in their life [1], cancer diagnosis has yet to leverage many of the advances made in the most modern of newer engineering and microfluidic technologies. Diagnosis often happens when the patient's cancer is already significantly advanced, despite the fact that time is one of the major factors in determining a patient's outcome. This diagnosis is also typically performed at a very large cost of both capital equipment and man-power. The possibility of reducing costs, reducing waiting times and enabling earlier detection of cancer by creating a method of detecting circulating tumour cells (CTC's) in a blood sample has been a goal of biomedical research for quite a long time. However, the isolation and identification of unique biological cells of interest from a large population of background blood cells remains a challenge in biomedical diagnostics and analysis [2–5]. CTC's may be present in concentrations of anywhere from one cell to a several thousand cells in a few mililiters of blood [6–8]. If the current hurdles to creating a point-of-care CTC detection device can be overcome there is an obvious application potential towards cancer screening and treatment [5, 9]. To that end, a lab-on-a-disc magnetophoretic device to detect the presence of CTC's was envisaged.

The initial concept of on-disc magnetophoresis for particle separation was presented in the conference proceedings of MEMS 2011 [10] and MicroTAS 2011 [11] by Siegrist *et al.*. Based on the success of this work, it was proposed that a device that could utilise the strengths of lab-on-a-disc magnetophoretic technology could be used to detect circulating tumour cells in a blood sample, and the advancement of this concept towards fruition is presented in the upcoming chapters of this document. Credit must be given to Jonathan Siegrist for initial work done on chapter two, in tandem with the author.

1.2 Cancer diagnostics

The field of cancer diagnostics has been at the forefront of biomedical research for many years and is a constant focus of new diagnostic devices and technologies. Currently, the most common way for a patient to be diagnosed with cancer of any type is to present to a doctor with physical symptoms. A positive diagnosis is usually only confirmed by either a biopsy or a scan, both of which are invasive and costly procedures (usually with long waiting lists) which often only diagnose the cancer too late to enable successful treatment. These procedures also require highly trained clinicians and technicians, which adds to the cost and time constraints accrued. A more recent addition to the cancer diagnostics field has been the area of circulating tumour cell detection. Circulating tumour cells have been known to exist since the late 1800s [12] and their responsibility for spreading cancer throughout the body via the circulatory system and causing metastases has been highlighted many times [13–15]. However, due to their incredibly high rarity in the blood [7, 8, 16], CTCs have not been accessible for diagnosis or prognosis until the advent of the Cellsearch system (Cellsearch, Veridax) in 2004, still the only FDA approved system for CTC detection. As well as costing many hundreds of thousands of dollars, the Cellsearch system has been shown to be very limited in its ability to reliably find and detect CTCs [16, 17]. There is therefore a gap in the market to develop a more reliable and financially agreeable CTC detection system that doesn't require a team of highly trained staff and a high-tech laboratory environment. If a patient could have a blood

sample taken and analysed in a point-of-care device in their doctor's office to show the presence of CTC's, then precious time and resources could be saved. Screening of the general public would be a far more realistic possibility and treatment outcomes could be determined by a blood sample. This would revolutionise cancer treatment.

1.3 The lab-on-a-disc platform

The field of centrifugal microfluidic or "lab-on-a-disc" platforms has been growing significantly in recent years and Ducrée, Burger, Stroheimer and Gorkin have all published excellent review articles on the topic [18–21]. The lab-on-a-disc platform enables liquids and particles to be controlled by the centrifugal force which is created by rotating the platform at the desired speed. The centrifugal force is a pseudo force that acts outwards from centre to edge from the frame of reference of the rotating disc [18].

While there have been numerous novel publications in the field of lab-on-a-disc platforms [18, 21, 22], this work focuses on the area of cell and particle control. The many advantages of the lab-on-a-disc platform for cell/particle analysis include precise control of sedimentation rates of cells or particles in liquid suspension by merely varying the centrifugal force through control of the rotation speed of the disc. The review by Burger *et al.* [19] focuses on this area in particular.

To enable rotation and visualisation of the microfluidic discs, a "spin-stand" instrument was used that allowed visualisation during rotation by means of a strobe light timed to the motor and optical setup [23] (Fig. 1.1).

This setup allowed for real time video of particle trajectories on the cellular level to be captured, which enabled a thorough analysis of cells or biomimetic polystyrene microparticles as they passed through the various microchannels on-disc. This process is outlined in greater detail along with an analysis of the various forces present for biomimetic particles in chapter two, while chapter three deals with advancing the work to enable using real cancer cells and blood on the platform.

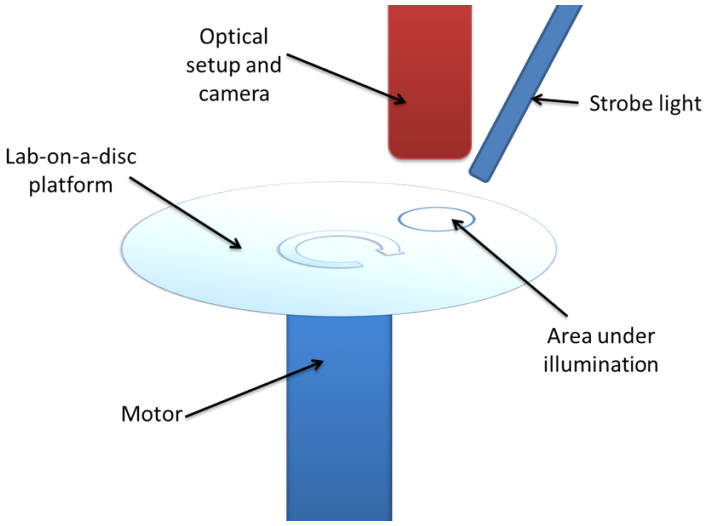

Figure 1.1: Schematic of the basic concept of the spin-stand. As the lab-on-a-disc platform spins, a strobe light is triggered once every rotation which allows the optical setup to obtain an image of the area under illumination. This enables real time visualisation of the disc during rotation.

1.4 Stopped-flow microfluidics

All microfluidic systems in this body of work are based on "stopped-flow microfluidics". Stopped-flow microfluidics consists of a microchannel filled with a stationary carrier fluid, through which particles or cells are sedimented by an external force.

This force could be gravity or the magnetic force. However, a unique advantage of centrifugal microfluidics is the fact that this force can be delivered and precisely controlled *via* the "artifical gravity" of the centrifugal force. This area of stopped-flow microfluidics on a centrifugal platform is almost completely unexplored. There are no papers more than ten years old in the literature on this topic. The first mention of a stopped flow system on a centrifugal platform is by Grumman *et al.*[25] and the only other published work which covered the area since then was by Burger *et al.* [24, 26, 27]. When trying to create new diagnostic platforms that analyse cells, bacteria, or any particulates that will sediment in a liquid, the stopped-flow centrifugal microfluidic platform offers many unique advantages (Fig. 1.2). These include,

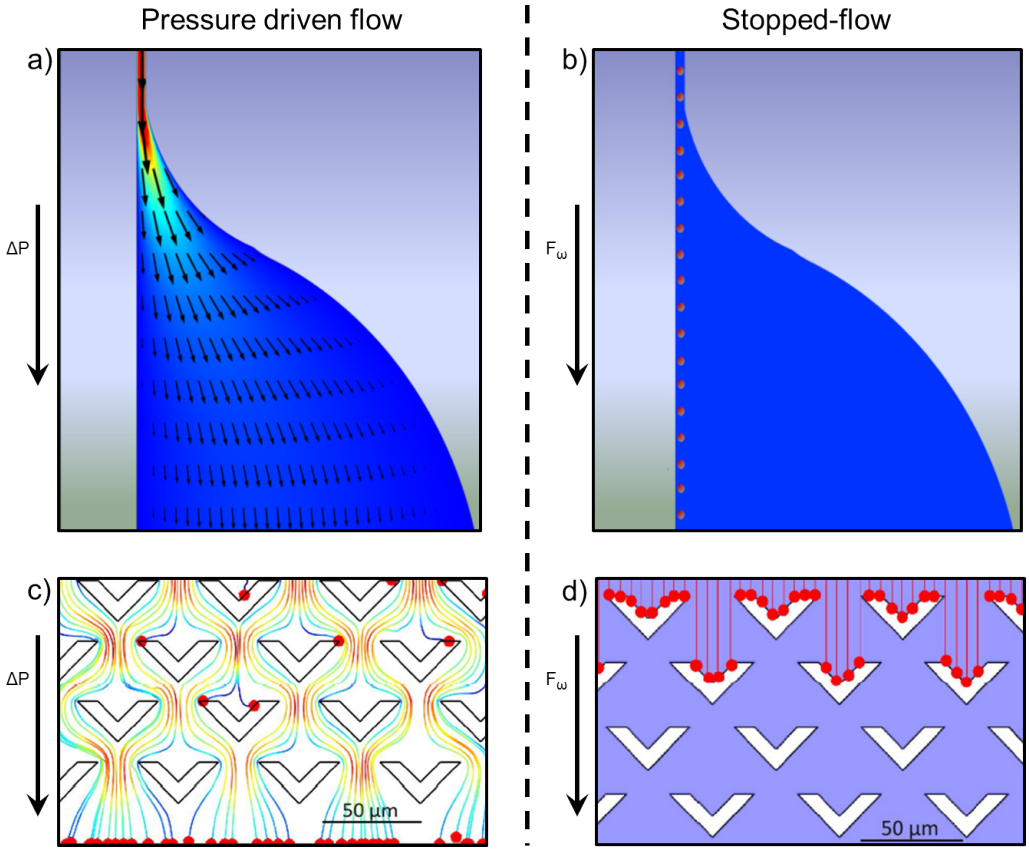

Figure 1.2: A comparison of the behaviour of a particle in a pressure driven flow-based system (left) and centrifugal stopped-flow system (right). a) A particle travelling in a moving liquid (due to a pressure difference ΔP) from a narrow channel into a wide channel will undergo a changing velocity profile depending on the channel width and will also follow the flow lines towards the centre of the channel (Comsol, USA). b) Whereas a particle sedimenting through a stationary fluid via the Centrifugal force (F_ω) will travel radially outwards, unaffected by the channel geometry. c) A flow-based system will cause most particles to follow the flow lines and travel around obstacles like the ones shown here [24]. d) Whereas in a stopped-flow system there are no flow lines and particles will merely sediment in a radially outward direction irrespective of any obstacles in their path [24].

but are not limited to, highly ordered particle motion (a unobstructed particle with a density greater than the liquid suspension will merely sediment radially outward in a straight line), precise velocity control by controlling spin rate, low-shear transport of cells due to the absence of fluid flow, uniform

velocity across a channel (parabolic flow profiles are not present), unique interaction parameters with obstacles in a chamber fig1.2 c& d , varying sedimentation rates depending on particle size and density for sorting purposes etc. etc.

While there are certainly caveats associated with stopped-flow microfluidics such as limitations on sample volume and loading difficulties (see chapter 5.2.4), it is an area of microfluidic research that should be thoroughly investigated to enable the exploitation of its unique parameters to create novel biomedical devices that will advance the field of lab-on-a-chip and point-of-care technologies.

1.5 Magnetic Particle Control

The majority of work presented in this thesis concerns the magnetic control of micro-particles or magnetically tagged cells on a rotating microfluidic platform. The field of magnetic particle control has been around for quite some time and has been reviewed extensively by Gijs *et al.* [28, 29] and Pamme *et al.* [4] and a very thorough and in depth analysis of all aspects of magnetic particle control, including particle manufacturing, an analysis of all forces present and a range of different magnetic particle handling platforms present in the literature can be found therein. These particles are also referred to as "beads" due to their spherical nature. The forces governing the motion of these magnetic (and non-magnetic) beads are dealt with in more detail in chapter two. However, a brief explaination will now be given.

One of the core principles of the centrifugo-magnetophoretic principle which is explored in this work is the separation of particles (cells or beads) of varying size, density and magnetic susceptibility. The three main categories are large non-magnetic particles ($10 - 20\mu m$), large magnetic particles ($10 - 40\mu m$) and small magnetic particles ($1 - 2\mu m$), represented in fig 1.3.

Under application of the centrifugal force on a microparticle suspended in a stationary fluid, particles will undergo sedimentation at a particular velocity. This velocity is dependent on many factors, the speed of rotation, the mass of the particle, the size and shape of the particle, the density difference

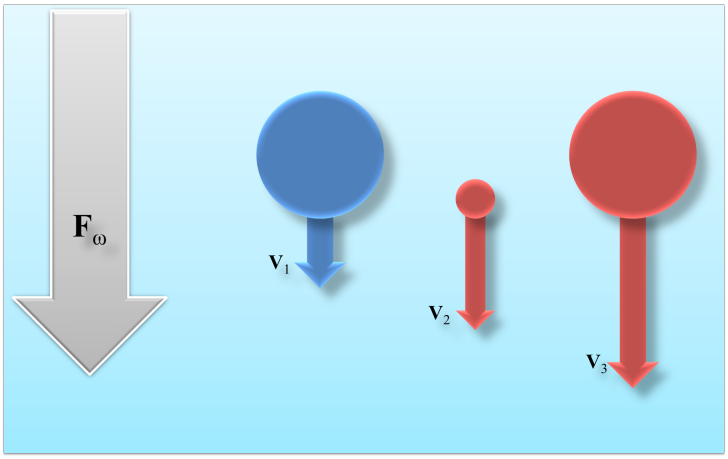

Figure 1.3: Under application of the centrifugal force on a microparticle suspended in a stationary fluid, those particles will undergo sedimentation. The relative velocities of three types of particles is indicated above. Non-magnetic polystyrene 20μm beads (blue) were the slowest, followed by the 1μm magnetic beads and finally the 20μm magnetic beads. The reason for this velocity difference is outlined in chapter 2.3.1.2

between the particle and fluid, and the viscosity of the fluid, to name but a few. These factors are all collected together to determine the three main forces which govern the particle motion. These are the centrifugal force (F_ω), the drag force (F_d) and, for magnetic particles, the magnetic force (F_m). A more in-depth analysis of these forces is given in chapter 2.3.1.

1.5.1 Superparamagnetic polymer beads

Superparamagnetic particles are single domain ferromagnetic nanoparticles which have zero magnetisation in the absence of a magnetic field due to their small size which allows their direction of magnetisation to flip randomly due to normal temperature fluctuations [30]. This gives the particles an overall average magnetisation of zero, unless an external magnetic field is present. The magnetic micro-beads used in this work are all of the superparamagnetic variety, that is, they are polystyrene micro-beads throughout which a dispersion of superparamagnetic nanoparticles are to be found (Fig. 1.4). The specific details of each type of particle used are given in the materials

and methods sections of the upcoming chapters. However, being superparamagnetic, the basic structure of the beads are all the same. For simplicity, superparamagnetic beads are simply referred to as "magnetic beads" in most of this work.

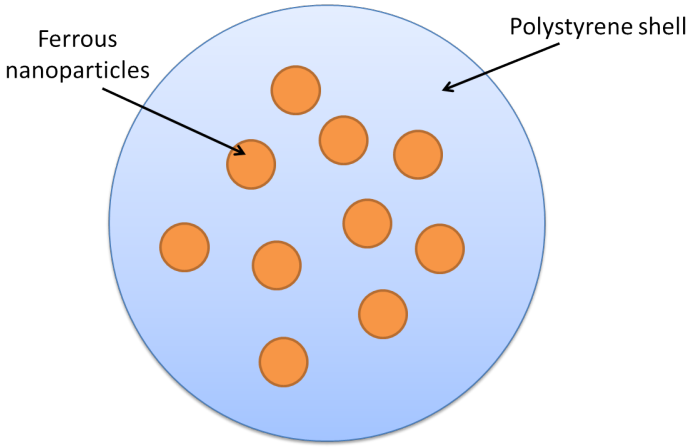

Figure 1.4: Superparamagnetic beads consist of a polystyrene bead throughout which a number of single domain superparamagnetic nanoparticles are dispersed. This allows the superparamagnetic effect to be created for a particle much greater in size than the typical superparamagnetic nanoparticle

1.6 Pseudo cells

Throughout this work, polystyrene microbeads were used as "pseudo cells" in order to prove the physical principle of cell separation and detection on the various platforms here-discussed before actual blood and cancer cells were then used. These polystyrene microparticles provide an excellent approximation of the behavious of cells in suspension on a centrifugal microfluidic platform. The polystyrene microparticles used for this work have a density of ($1050\text{Kg}/m^3$) which is very close to that of an actual blood cell or cancer cell in blood $1080 \pm 5\text{Kg}/m^3$ [31]. And a superparamagnetic microbead of 10-20μm very closely approximates the behaviour of a cell that has been tagged with numerous 1μm magnetic beads (Fig 1.5).

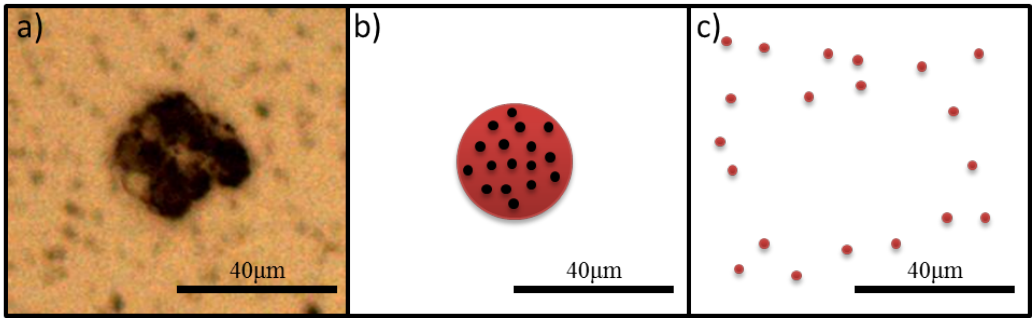

Figure 1.5: a) Microscope image of a cluster of MCF7 breast cancer cells that are coated with many 1μm magnetic beads, resulting in the dark black/brown colour. b) A schematic of a superparamagnetic polystyrene microparticle of the same size as the cell cluster. The black dots represent the magnetic nanoparticles within the microparticle. c) The red dots represent the unbound 1μm beads that can be seem in the background of (a). They are composed of the same nanoparticle interior as the larger particle in (b).

A calculation of the iron content of a 20μm magnetic bead (Microparticles, GmbH) and an MCF7 cell coated with 200 1μm magnetic beads (Microparticles GmbH) was undertaken to determine how accurate this approximation was. Based on the percentage of ferrous content (20% by volume) given by the supplier, a 20μm magnetic bead was found to have a mass of 3.12x10^{-12}Kg of ferrous material in each bead. When compared to a MCF7 cell cluster in fig 1.5 with approximately 200 1μm magnetic beads on its surface, the total mass of ferrous material on the surface of the "tagged cell" was found to be 4.81x10^{-13}Kg. It was felt that this was close enough to assume that a 20μm magnetic bead would provide a reasonable approximation of the behaviour of a magnetically tagged MCF7 cell.

The beads also had the advantage of having highly homogeneous properties and being very easy to visualise on the spinstand and microscope. This enabled quick and accurate tests and calculations to be carried out before moving on to the more complex biological samples of blood and cancer cells.

Chapter 2

Centrifugo-Magnetophoretic Particle Separation

This chapter is based on the following publication:
Centrifugo-magnetophoretic particle separation,
Daniel Kirby, Jonathan Siegrist, Gregor Kijanka, Laetitia Zavattoni, Orla Sheils, John OLeary, Robert Burger and Jens Ducrée,
Microfluidics and nanofluidics 13.6 (2012): 899-908.

Before a fully functional CTC detection device with integrated sample-prep, cell isolation and on-board detection could be envisaged, it was necessary to first prove the physical principle of centrifugal-magnetophoresis. Once this was done, the door would be opened for the manifold potential applications for stopped-flow magnetophoretic separations of cells, proteins, and nucleic acids in bioanalytics, cell biology, and clinical diagnostics. To ensure stable hydrodynamic conditions and thus reproducible separation, state-of-the-art magnetophoretic lab-on-a-chip systems have been based on pressure-driven flow [2–4], which involves rather bulky and costly instrumentation. In a flow-based system, suspended particles are following the liquid phase as a result of the Stokes drag, thus being fully exposed to divergent flow lines around obstacles and pump-induced pressure fluctuations. In order to eventually achieve more stable hydrodynamic conditions, improved control of magnetic particles, a more compact instrumentation footprint, and integration of high-performance upstream sample preparation, this chapter introduces the novel 2 dimensional particle separation principle (centrifugal-magnetophoresis) by combining magnetic deflection with centrifugal sedimentation in a stopped-flow mode (i.e., mere particle sedimentation). The experimental parameters governing our centrifugo-magnetophoretic system are the strength and orientation of the co-rotating magnetic field, the rotationally-induced centrifugal field, and the size-dependent Stokes drag of the various particles with respect to the (residual) liquid phase. In this work, the following set of basic functional modes is demonstrated as proof-of-concept: separation of magnetic from non-magnetic particles, routing of magnetic particles based on control of the spin speed, and size separation of various magnetic particles. Finally, a biomimetic application involving the separation of particles representing healthy cells from a very small concentration of magnetic particles of a similar size, mass and magnetization as a immuno-magnetically tagged target cell.

2.1 Introduction

While large, automated systems, such as fluorescence and magnetically-assisted cell sorters (FACS and MACS, respectively), have been successful in analysis of cells, their associated instrumentation and operation proves to be bulky, complex, and expensive [5]. Thus, the development of smaller-scale, microfluidic cell capture and isolation systems remains of high interest. Such systems would benefit from the commonly quoted advantages of microfluidics (e.g., high amenability to automation, process integration, multiplexing and parallelization, substantially reduced sample and reagent volumes, smaller instrument footprint, portability, low costs of ownership) while possibly gaining additional functionality over current macrofluidic systems [32, 33]. However, proof-of-concept of such a system will only transfer into useful applications if it can be integrated with upstream sample preparation [34] to form a full-fledged sample-to-answer technology. In the case of rare cell detection from whole blood, the platform utilized must also be able to process and handle the comparatively large blood-sample volumes in a low-loss fashion to obtain statistically representative counts of these bioparticles [9]. A common, general method for biological separation is the linking of analytes with particles/beads, followed by the subsequent control and separation. This continues to be a feasible approach to the problem, and has already found widespread commercial applications using magnetic particles [2, 5]. Smaller-scale systems have also been developed, including microfluidic continuous-flow and magnetophoretic systems [2, 3, 35, 36]. To date, practically all continuous, microfluidic separation systems have been flow-based, pressure-driven systems. However, such implementations exhibit inherent disadvantages. Initial particle focusing is an issue, as the microparticles tend to follow divergent flow lines to compromise resolution [37]. Moreover, pressure-driven systems, while providing good control at larger flow rates, tend to be difficult to manage at low flow rates, which are required for microparticle control and focusing [18, 21, 38, 39]. In an effort to overcome these disadvantages, this work adapts a magnetophoretic system onto a rotational lab-on-a-disc platform operating in stopped-flow mode. The centrifugal, ar-

tificial gravity force propels particles through a stagnant carrier fluid and separates/routes them according to their density, size, and magnetic properties in the presence of a co-rotating, permanent magnet polarized in a direction perpendicular to the centrifugal force. Apart from the elimination of (divergent) flow lines, obvious advantages are gained with the centrifugal system as compared to common pressure-driven schemes, including the simple, cost-efficient, low-maintenance instrumental setup (CD player), the ease-of-handling of the disc-shaped substrates (CDs or "discs") that do not require tubing interconnects, and the freely-programmable and inertially-stabilized, jitter-free centrifugal actuation mechanism that features a large force range and a rotationally-symmetric field for facile parallelisation [18, 21, 39, 40].

2.1.1 System concept, design, and advantages

In this chapter, we describe a magnetophoretic system inspired by the concepts of Pamme and Manz [3] that was for the first time adapted onto a centrifugal microfluidic platform towards cell separation applications. The device works by centrifugally sedimenting particles in a stagnant carrier fluid through a magnetic field generated by disc based permanent magnets (Fig. 2.1).

The novel, 2-dimensional, centrifugo-magnetophoretic system is governed by the interplay of several experimental control parameters and forces as follows: rotational spin-speed (controls centrifugal field), particle size and viscosity of the carrier fluid (affects Stokes drag), particle density (impacts sedimentation rate), and the geometry of the separation chamber (controls, for instance, particle residence time and magnetic field distribution). Moreover, the strength, position, and orientation of the co-rotating permanent magnet can also be customized. The entire system (Fig. 2.2) is first primed with liquid. Next, a particle suspension is introduced to the loading chamber. After mounting of the on-chip permanent magnet, the hybrid, microfluidic disc is placed on a spin-stand motor and rotated at various speeds to centrifugally sediment and separate/route the particles. The particles first enter the focusing channel where they are aligned along the wall distant to the magnet

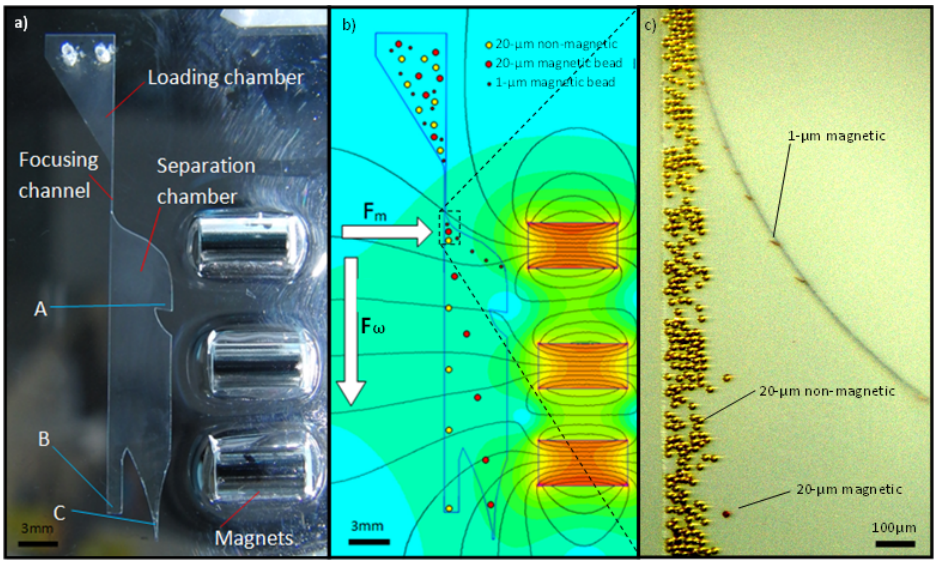

Figure 2.1: a) Photograph of a single centrifugo-magnetophoretic separation device on the disc with relevant features labeled. b) Schematic and magnetic model showing the separation forces present in the system with calculated trajectories and destinations of 3 different particles. The centrifugal force Fω and the magnetic force Fm are also displayed, with magnetic field intensity being represented by a colour gradient. Magnetic modeling was done with the program FEMM-finite element method magnetics. c) Image of three-way separation of beads at the opening of the separation chamber as outlined in the schematic. 1μm particles have formed trains along the field lines and are therefore visible as long streaks, not individual spheres.

(Fig. 2.1). Upon leaving the focusing channel, magnetic particles are immediately deflected towards the permanent magnet near the opposite sidewall of the separation chamber. Depending on the spin speed and their size, the magnetic particles either arrive in the capture notch A or the collection reservoir C. In contrast, all non-magnetic particles sediment on straight, radial trajectories through the separation chamber into reservoir B (Fig. 2.1).

It is worth emphasizing again that sedimentation occurs without flow; particles merely sediment through the stationary carrier fluid, therefore eliminating impairment of the separation resolution caused by divergent flow lines and hydrodynamic instabilities. Thus, if these magnetic and non-magnetic particles are mixed and introduced simultaneously, they can easily be spa-

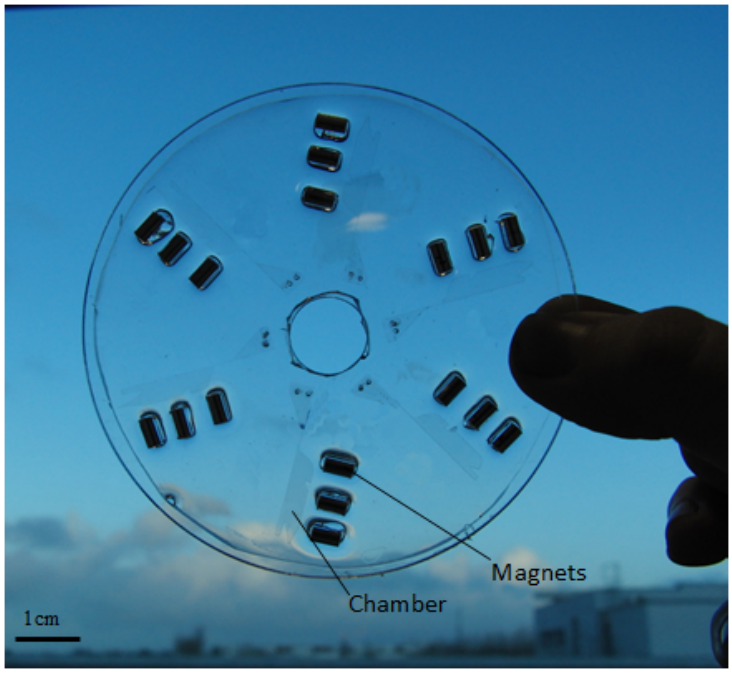

Figure 2.2: Photograph of entire disc, showing six microfluidic chambers with three magnets parallel to each chamber. The magnified views of the individual chambers can be seen in Fig. 2.1.

tially separated, even under low hydrodynamic or mechanical stress (e.g. compared to just holding a permanent magnet against the outer wall of the vessel). Within the wide spectrum of possible system designs and operational parameters, this proof-of-concept strategy reports on a specific geometrical layout that was chosen to display several basic functional modes of the centrifugal magnetophoretic system. In this work, silicone discs are fabricated and tested to first show separation of magnetic from non-magnetic particles. Next, separation of different sizes of magnetic particles is shown, followed by routing of a fixed type of magnetic particle to a designated location controlled by the rotational spin-speed. Finally, we present a 3-fold differential separation of a mixture of non-magnetic particles and magnetic particles of different sizes. This particle separation may be regarded as biomimetic of an actual sample of untagged cells, magnetically tagged cells and excess tagging particles.

2.2 Materials and Methods

2.2.1 Device fabrication

The microfluidic devices were designed in AutoCAD (Autodesk, Inc., CA, USA) and fabricated out of polydimethylsiloxane (PDMS) (Sylgard 184, Dow Corning; #101697, Farnell, UK) using standard SU-8 soft-lithography processes [41, 42]. A two-level, SU-8 mold was created on a bare, 4 inch Si wafer by first spinning on SU-8 3050 (Microchem, MA, USA) to a thickness of 100μm; this first layer formed the focusing channels and separation chambers (Fig. 2.2). The second SU-8 layer was spun on to a thickness of 150μm and formed the loading chambers. Baking, UV exposure, and developing steps were performed separately for each layer according to the manufacturers recommendations. Note that each disk contains 6 identical separation structures. After creation of the SU-8 mold, it was cleaned using UV/ozone for 5 minutes and then silanized using octadecyltrichlorosilane (#O5877, Sigma-Aldrich, IE) vapors for at least 4 hours to promote PDMS release. To prepare the PDMS, Sylgard 184 curing agent and base were mixed in a ratio of 1:5 by weight, degased, poured over the SU-8 mold, degased again until all bubbles were eliminated, and then cured in an oven at 70°C for 1 hour. The PDMS part was removed from the mold, and holes, including the center hole, loading holes, and permanent magnet holes, were punched and cut out from the disc manually. Next, stock 2-mm thick polymethylmethacrylate (PMMA) (#824-632, Radionics, IE) was laser cut into a standard CD format (10-cm diameter) and cleaned using isopropanol and DI water. Sylgard 184 curing agent and base, mixed this time in a mass ratio of 1:20, was mixed, degased, and spun onto the PMMA disc at 1500 revolutions-per-minute (RPM). The PDMS-coated disc was then cured in an oven at70°C for 1 hour. Finally, the PDMS microfluidic device, with pre-cut holes, was manually aligned to the PDMS-coated PMMA base. The PDMS-to-PDMS bond was enabled by the mismatch in the concentrations of the curing agent [43], thus forming a practically irreversible bond between the PDMS layers. Adhesion between

the spun-on PDMS and clean PMMA disc was completely leak-proof at the spin-speeds used in these experiments.

2.2.2 Spin-stand instrument

To run the separation experiments, a servo-motor coupled to a stroboscopic visualization system similar to that already described in Chapter 1.3 was used for particle flow and tracking during rotation. A servo-motor (4490 series, Faulhaber, DE) was mounted to a framed support, and a custom chuck was machined for securely attaching standard discs to the servo-motor shaft. A CCD camera (Sensicam series, PCO, DE) was placed directly above the motor, and a combination of optical components (Navitar, NY, USA) and controls for particle visualization were attached to the camera to obtain a microscopic image; the optical setup also included a motorized zoom and focus to allow for multi-scale imaging of features on the microfluidic device. A linear drive was used to radially position the camera along the disc. The camera was triggered to capture one frame per rotation, such that a movie composed of a sequence of still images taken at the same location on the disc could be acquired. A custom control box was fabricated to handle triggering between the motor, camera, and stroboscopic illumination system; the trigger box also served to control the circumferential location along the disc for image acquisition. The combined action of the linear camera drive and the trigger box provided full control to select the desired sector of the disc to be investigated and imaged. The stroboscopic system (Drelloscop 3244, Drello, DE) utilized a liquid light-conductor for illumination and was mounted above the disc and to the side of the camera. A desktop PC (Dell, US) was used to control the spin-speed and sequences of the motor as well as for monitoring and image acquisition. The custom spin-stand instrument allowed for real-time movement and magnification such that the flow of particles through the microfluidic device could be tracked. The optical clarity of the PDMS and PMMA device components, the bright stroboscopic illumination as well as coloring of the particles (see figure 2.3) provided adequate contrast for visualization.

2.2.3 Particle separation experimental materials

Various types of particles were sourced for characterizing the centrifugal-based magnetophoretic system. The particles used included polystyrene particles ($d = 20\mu$m; $\rho \approx 1.1 g cm^{-3}$; #PS, MicroParticles, GmbH, DE), and iron-core, paramagnetic polystyrene particles of two different sizes ($d = 1.43\mu$m and 18.8μm; $\rho \approx 1.7 g cm^{-3}$; #PS-MAG-S1792, #PS-MAG-S1985, and #PS-MAG-S1986, MicroParticles, GmbH, DE). The polystyrene particles were yellow and the magnetic particles were red; this allowed for easy visualization and differentiation on the spin-stand instrument and under the bright-light microscope. Particle sizes will be referred to as 20μm (magnetic and non-magnetic), and 1μm (magnetic) for convenience. All particles arrived as either 5% or 10% w/v solutions. After vortexing and/or sonication to homogenize the suspensions, dilutions of each particle type were made through a 1:10 ratio of particles to medium. The dilution medium consisted of PBS (phosphate buffered saline, 0.1 M phosphate buffer, 0.0027 M potassium chloride and 0.137 M sodium chloride, pH 7.4) with 0.1% BSA (bovine serum albumin). All particle mixtures were vortexed briefly before introduction to the disc.

2.2.4 Biomimetic separation experimental materials

For the biomimetic cell separation experiments (as already described in chapter 1.6), red, 20μm magnetic particles were used to mimic cells of a similar size, mass and iron content which are coated with several hundred biofunctionalized 1μm magnetic beads. Background, i.e. untagged blood cells were represented by 20μm polystyrene particles as they were of a similar mass as blood cells and exhibit a different colour to the magnetic particles. Finally, a real-world analytical sample would exhibit excess tagging particles, in this case 1.43μm, magnetic iron cored polystyrene particles. These were also included in the sample to give a more realistic biomimetic blood sample of 20μm polystyrene beads, 20μm iron cored polystyrene beads and 1μm iron cored magnetic beads. This sample was then processed through the

centrifugo-magnetophoretic system and 3-way separation was observed as will be discussed in section 2.3.

2.2.5 Experimental protocol and data analysis

After assembly and fabrication (see section 2.1), the microfluidic disc (Fig. 2.2) was primed with an excess (50μL) of solution using degas-driven flow [44] and then placed onto the spin-stand instrument. Nickel-plated, rod-shaped permanent magnets made of NdFeB (3 mm diameter, 6 mm long) (S-04-10-AN, SuperMagnete, DE) were mounted on the disc. Next, 3μL aliquots of the various microparticle mixtures were placed in the loading chamber and then centrifugally sedimented through the system; spin speeds in the range of 225 RPM to 750 RPM were evaluated. A spin speed of 420 RPM (7Hz) was found to feature optimum separation of particles. The trajectories of the deflected particles were monitored using the stroboscopic imaging system described above and total number of particles trapped in each area was calculated using the theory of random loose packing [45] where the captured number of particles was large, and counted under an optical microscope where the number was small (roughly less than 20) and easily visible. Particle deflection/separation was quantified by calculating the percentage of particles that ended up in each of the three chambers with the 1μm magnetic beads to go in to chamber A the 20μm non-magnetic beads to go into chamber B and the 20μm magnetic beads to go into chamber C (Fig. 2.3).

2.2.6 Magnetic modeling and measurements

To initially optimize the position and properties of the on-disc permanent magnet, we simulated the magnetic fields for various types and positions of permanent magnets (Fig. 2.1b) with the software package FEMM (Finite Element Method Magnetics 2010). It was found that magnets producing a high magnetic field gradient would be needed for this system, and so NdFeB magnets were chosen. It was also determined that 3 rod-shaped magnets ($3mm$ diameter, $6mm$ long) placed at a distance of approx. $2.5mm$ from the side and staggered along the length of the separation chamber would exhibit

a suitable magnetic flux density and field strength of $130mT$. Furthermore, the magnetic field gradient (as a gross linear approximation) amounted to roughly $50mTmm^{-1}$. The positioning of the magnets was selected by educated guess initially and then further optimized empirically. To validate the simulation results, the magnetic field was also measured using a Gaussmeter (#CYHT201, Chen Yang Technologies, DE). We measured a magnetic field strength of $100mT$ and a magnetic field gradient (again as a gross linear approximation) of 30 $mTmm^{-1}$, correlating well with the modeled data.

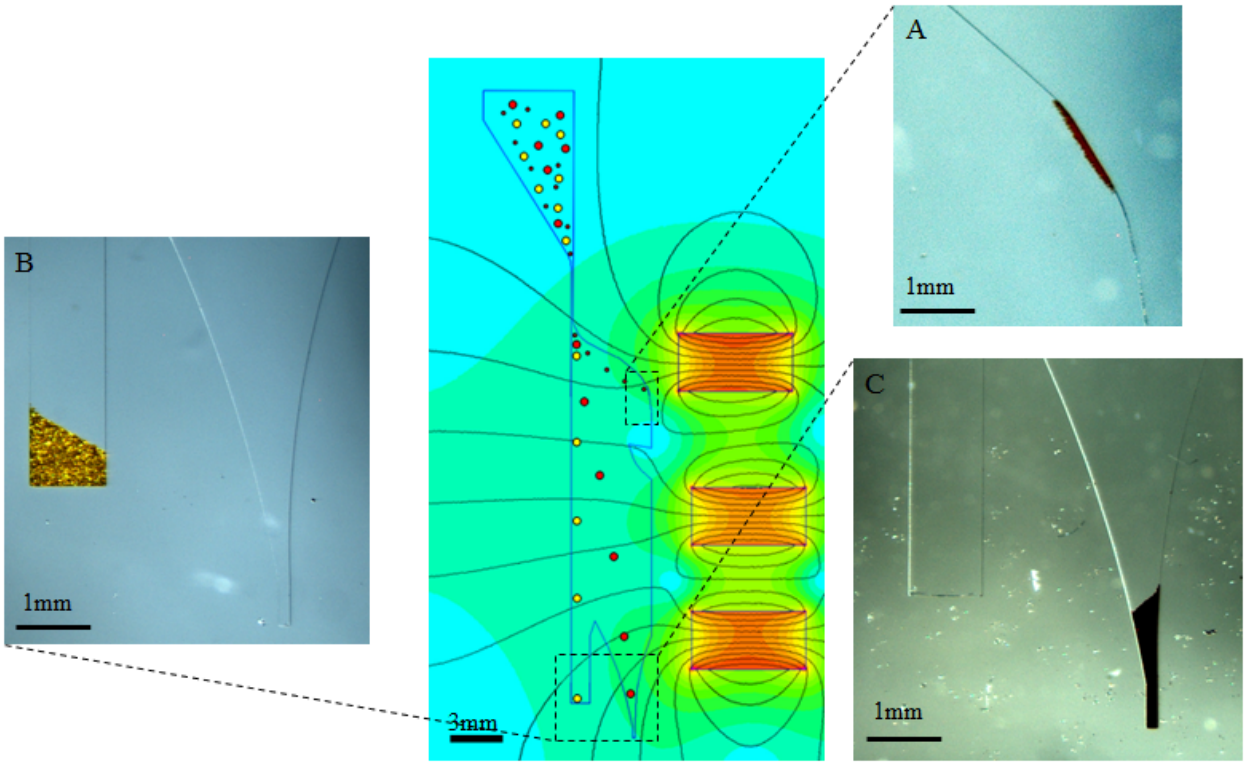

Figure 2.3: Images of captured particles from three separate experiments where 100% of the beads went to their intended capture areas. Capture area A: 1μm magnetic beads were deflected strongly due to their slow sedimentation speed and 100% trapping was observed. Capture area B: 100% of the 20μm non-magnetic beads were recovered. Capture area C: Again, 100% of the 20μm magnetic particles were retrieved.

2.3 Results and discussion

The work described in this chapter focuses on the general introduction of the fundamental concept of centrifugo-magnetophoretic separation. A preliminarily optimized, fixed magneto-microfluidic system configuration was chosen from a wide range of possible layouts to demonstrate various basic functional modes of the system. Experimental results from the solely particle-based experiments are first presented (Fig. 2.4), showcasing magnetophoretic separation capabilities of our novel system along with considerations of the relative forces involved. Finally, the results of biomimetic experiments are highlighted, showing the high potential for real-world applications (Fig. 2.5).

2.3.1 Particle-based results and discussion

We start this section with a brief description of the forces present in this system to leverage the interpretation of the subsequently presented experimental results and functional modes.

2.3.1.1 Separation forces

Particle motion in the system is governed primarily by the centrifugal (F_ω), magnetic (F_M) and velocity-dependent Stokes drag (F_D) forces. At elevated particle speeds (relative to the disc), the rotational Coriolis force (F_C) also plays a role in the particle routing mechanism. Briefly, the Coriolis force, which acts in the same plane as the disc, forces particles in a direction perpendicular to that of the centrifugal force and opposite to that of the direction of rotation. In fact, for a sufficient magnitude at high sedimentation speeds, the Coriolis force may artificially enhance or counteract the observed magnetic deflection/routing. The relative strengths of the forces acting on a single magnetic particle can be estimated based on known and observed characteristics of the platform in combination with the results obtained from the magnetic modeling and measurements. The following equations describe the magnitudes of the four forces present in the system:

$$\vec{F}_{\omega} = \Delta\rho \; d \; \omega^2 \tag{2.1}$$

$$\vec{F}_m = \frac{V_p \, \Delta\chi}{\mu_0}(\vec{B} \cdot \nabla)\vec{B} \tag{2.2}$$

$$\vec{F}_m = \frac{V_p \, \Delta\chi}{\mu_0}\begin{pmatrix} B_x\frac{\partial B_x}{\partial x} + & B_y\frac{\partial B_x}{\partial y} + & B_z\frac{\partial B_x}{\partial z} \\ B_x\frac{\partial B_y}{\partial x} + & B_y\frac{\partial B_y}{\partial y} + & B_z\frac{\partial B_y}{\partial z} \\ B_x\frac{\partial B_z}{\partial x} + & B_y\frac{\partial B_z}{\partial y} + & B_z\frac{\partial B_z}{\partial z} \end{pmatrix} \tag{2.3}$$

$$\vec{F}_d = 6\pi\eta r_0 \nu \tag{2.4}$$

$$\vec{F}_c = 2\Delta\rho\omega\nu \tag{2.5}$$

where $\Delta\rho$ is the density difference between the particle and the liquid, d its distance from the particle center to the center of the disc, ω is the angular frequency of the disc rotation, $\Delta\chi$ is the difference between χ_P and χ_M, the magnetic (volume) susceptibilities of the particle and the medium, respectively, V_P is the volume of the particle, B is the magnetic flux density that arises from the on-chip permanent magnet, μ_0 is the vacuum permeability constant ($1.2566x10^{-6} VsA^{-1}m^{-1}$), η is the viscosity of the carrier fluid, r_0 is the radius of the particle, and ν is the velocity of the particle [3, 18]. Equation 2.3 is the expanded form of equation 2.2. For the purposes of these calculations, a 20μm magnetic particle with a density of $1.9 gcm^{-3}$ is located at the side of the separation chamber closest to and radially aligned with the magnet (at a distance from the center of rotation of about 35 mm). It is worth noting that a particle at this position experiences a maximum magnetic force, and a measured magnetic flux density on the order of $100mT$ with an approximate linear gradient of around $30mTmm^{-1}$ which was used for the calculations. The magnetic (volume) susceptibility of the particle is assumed to be on the order of 0.15 (dimensionless) based

on previous publications, and water is the carrier fluid [3]. At a spin speed of $420RPM$ a mean particle sedimentation velocity of $137 \pm 12.6\mu ms^{-1}$ was experimentally observed using Tracker video analysis and modeling software (http://www.cabrillo.edu/ dbrown/tracker/) over 4 experiments. Based on these assumptions, an estimation of the strength of the forces acting on a single magnetic particle in the x direction (towards the magnet) is obtained as follows:$f_M = 1,500pN$, $f_\omega = 480pN$, $f_D = 26pN$, and $f_C = 0.09pN$. Thus, the predominant forces are the magnetic and the centrifugal forces, while the Stokes drag and Coriolis forces are less prevalent. To better understand the increased ratio between the two dominant forces ($f_M/f_\omega = 3.1$) in view of the rather moderate deflection angles observed, one must consider the transient nature of the magnetic force as experienced by the particle. While the centrifugal force is unidirectional and high in magnitude along the entire radial length of the separation chamber (about 20 mm), the particle experiences strong, lateral magnetic-force components only when in close proximity to the magnet; this strong magnetic force is thus experienced throughout a radial travel distance roughly corresponding to the width of the permanent magnets (3 mm). These crude approximations provide a 3.1-fold higher magnitude and a 6.7-fold reduced interaction interval of the magnetic force with respect to the centrifugal force. Thus, it can be concluded that in the time-average over the two forces, their effective impact on the particle trajectory is comparable and can therefore be utilized to fine-tune the routing of magnetic particles through the separation chamber.

2.3.1.2 Particles' terminal velocity

The calculations for particle velocity in the previous section were carried out using an experimentally observed velocity to determine the drag force due to the particle velocity at that point in time. There are inherent complications in calculations such as these due to the velocity change of the particle with respect to time. It was therefore thought important to carry out calculations to determine the terminal velocity of particles of two different sizes in order to explain the velocity difference between the slow 1μm beads and the

much faster 20μm beads. This can easily be explained by the analogy of the terminal velocity of an object falling to earth under the gravitational force. At terminal velocity, the acceleration of the object will go to zero and the viscous drag force from the air will be equal to the gravitational force on the object. This analogy is precisely the same for the microparticles sedimenting through the stagnant fluid. At terminal velocity the viscous drag force on the microparticle f_D will equal the centrifugal force f_ω on the microparticle and this allows for a calculation of the terminal velocity to be undertaken. The terminal velocity of a 1μm magnetic bead at a distance of 35mm from the disc centre was found to be 0.22μm/s and the terminal velocity for a a 20μm magnetic bead at the same location was found to be 39μm/s. This clearly explains the observed velocity difference between the particles, even though the 1μm particles were slightly more dense due to a higher iron content.

2.3.1.3 Separation of magnetic from non-magnetic particles

The fundamental capability of centrifugo-magnetic separation is first demonstrated in its most simple variant, the capture of 20μm non-magnetic beads, 20μm magnetic beads and 1μm magnetic beads in three separate capture areas at a spin rate of 420 RPM (Fig. 2.3). As already discussed, the selective routing of the beads to designated capture zones roots in the specific interplay of the centrifugal force f_ω, magnetic force f_M and the Stokes drag f_D. The non-magnetic particles simply follow f_ω to sediment straight down the channel. The 20μm magnetic beads are additionally impacted by f_M to laterally deflect them into capture area C. And finally, the 1μm magnetic beads (despite having a slightly higher density than the 20μm magnetic beads) sediment at a considerably lower velocity due to the ratio of centrifugal to viscous forces being proportional to r^2 [29] and thus experience a greater deflection by the lateral magnetic field f_M into the capture area "A" due to their increased time in the magnetic field and slightly higher iron content(Fig. 2.3). The next stage was the separation of magnetic from non-magnetic particles. To this end a mixture of magnetic and non-magnetic polystyrene particles

of similar size ($\approx 20\mu$m in diameter) were processed at a spin speed of 420 RPM for about 20 min.

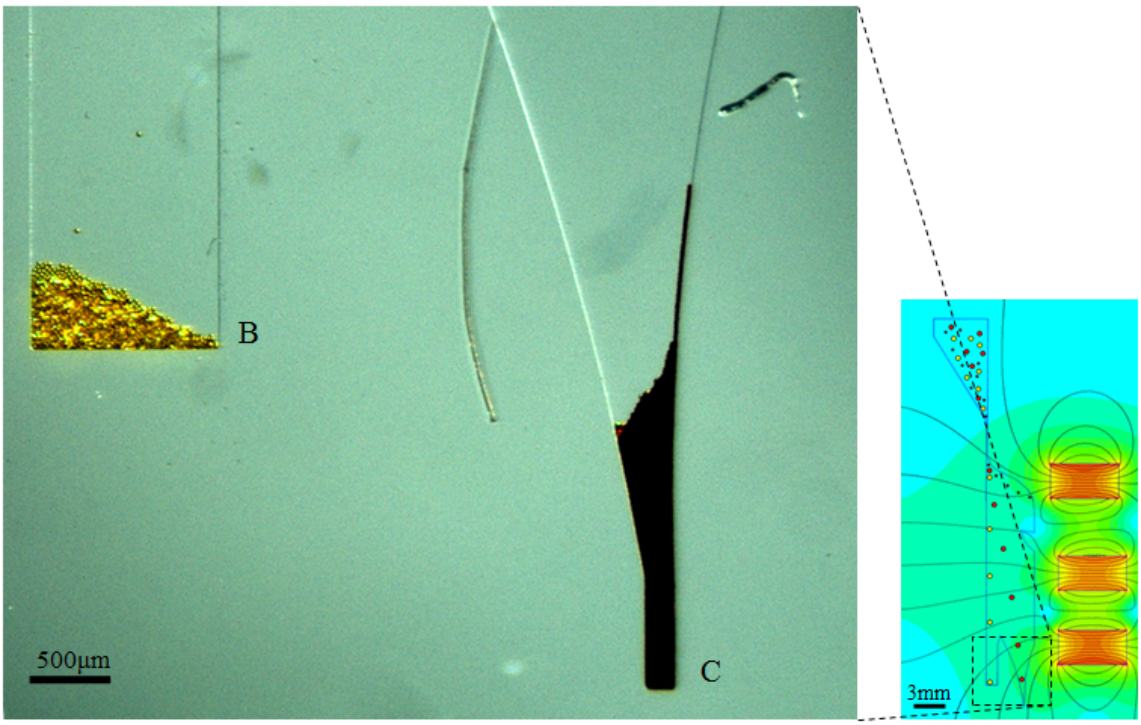

Figure 2.4: After introduction of a mixture of yellow, 20μm non-magnetic beads and red, 20μm magnetic beads into the loading chamber, the system was spun at 420 RPM. A complete, 100% separation of the beads was observed.

The results in Fig. 2.4 feature an excellent degree of accuracy and exhibit 100% separation of 20μm non-magnetic from 20μm magnetic beads. The next mixture of particles separated was 20μm non-magnetic beads and 1μm magnetic beads. Both types of beads followed the same pathway as they did when run separately through the system (Fig. 2.3) with 100% of non-magnetic 20μm beads captured ending up in capture area B and 100% of 1μm magnetic beads captured ending up in capture area A. The initial branching of the bead trajectories upon entering the separation chamber in (Fig. 2.1c) shows the 1μm beads forming trains of beads as they line up along the magnetic field lines [46] and deflecting to the right-hand magnets, with the 20μm non-magnetic beads continuing radially outwards.

It should be mentioned that the Coriolis force f_C may to a small extent artificially enhance the observed magnetic separation. However, we selected the of rotation such that f_C counteracts f_M, thus preventing an enhancement of the lateral deflection. So the experimental results obtained on the here presented choice of the centrifugo-magnetophoretic system design with the specified control parameters provide clear evidence for capability of particle focusing and separation.

2.3.2 Biomimetic separation results and discussion

The final set of experiments was performed to mimic the realistic conditions of extremely rare CTCs suspended in the blood stream. Typically, one CTC would be present in a background of roughly a million white blood cells and a billion red blood cells. Our biomimetic sample consisted of a very high concentration of 20μm polystyrene beads ("pseudo blood cells") spiked with a minute concentration of 20μm magnetic beads ("psuedo magnetically tagged rare cells") and a high concentration of 1μm beads (excess, i.e. unbound magnetic tagging beads). Note that at this pioneering stage of our research the CTC-to-blood-cell ratio chosen is still significantly higher in our biomimetic sample than in a patient blood to avoid problems with the otherwise required handling of large-scale, milliliter volumes on miniaturized lab-on-a-chip system. The final test consisted of 5 runs with an average content per run of $\approx 16,300$ non-magnetic beads (20μm, i.e. mimicking non-target cells), ≈ 37 magnetic beads (20μm, i.e. mimicking tagged target cells) and $\approx 700,000$ magnetic tagging beads (1μm, i.e. mimicking unbound magnetic tags).

These samples were separated with extremely high selectivity (Fig. 2.5 & table 2.1). It was observed over the 5 runs that $96.3 \pm 11.2\%$ of the 20μm magnetic particles (representing CTCs) were captured in the correct terminus C, there were only a small fraction (3.7%) of false negatives (CTCs in B) and less than 0.1% false positives (regular blood cells in C).

While this level of error is very small, it would be an unacceptable amount of error if the system were scaled up to handle realistic CTC concentrations. The reason for the error was observed to be non-specific binding of a non-

Capture area	20μm non-magnetic	20μm magnetic	1μm magnetic
A	3(0.02%)	0(0%)	7.1×10^5(100%)
B	16, 344(99.93%)	1.4(3.7%)	0(0%)
C	9(0.05%)	36(96.3%)	0(0%)

Table 2.1: Statistical data from n=5 runs of 3-way particle separation

magnetic bead (regular blood cell) to a magnetic tagging bead and its resulting routing into chamber C. This issue may possibly be resolved by suitable optimization of bioanalytical immuno-binding and blocking strategies.

2.4 Conclusion and outlook

In this work, a novel centrifugo-magnetophoretic platform for particle separation was conceptually introduced and experimentally investigated. According to their physical properties, such as size and magnetization, the distribution of the magnetic field, and the freely-programmable spin speed, the platform is capable of routing microparticles into one out of three available outlets. For a chosen system configuration, a set of basic functional modes was investigated using a range of particle types and rotational frequencies. In this proof-of-concept study, prospective cell separation capability was evaluated by biomimetic experiments utilizing particles of similar mass, size and magnetization as target and background cells as well as an abundance of 1μm magnetic tagging particles. The main advantages of the simple and robust platform are the very stable hydrodynamic conditions in the centrifugally enabled, jitter-free, stopped-flow mode which is unique to the centrifugal platform. The results of these tests enabled the work to move on to more advanced biological cell separation, as show in figure 2.6 and described in the upcoming chapters.

As established in the literature, the centrifugal microfluidic platform is also well-amenable for powerful sample preparation, including classic meth-

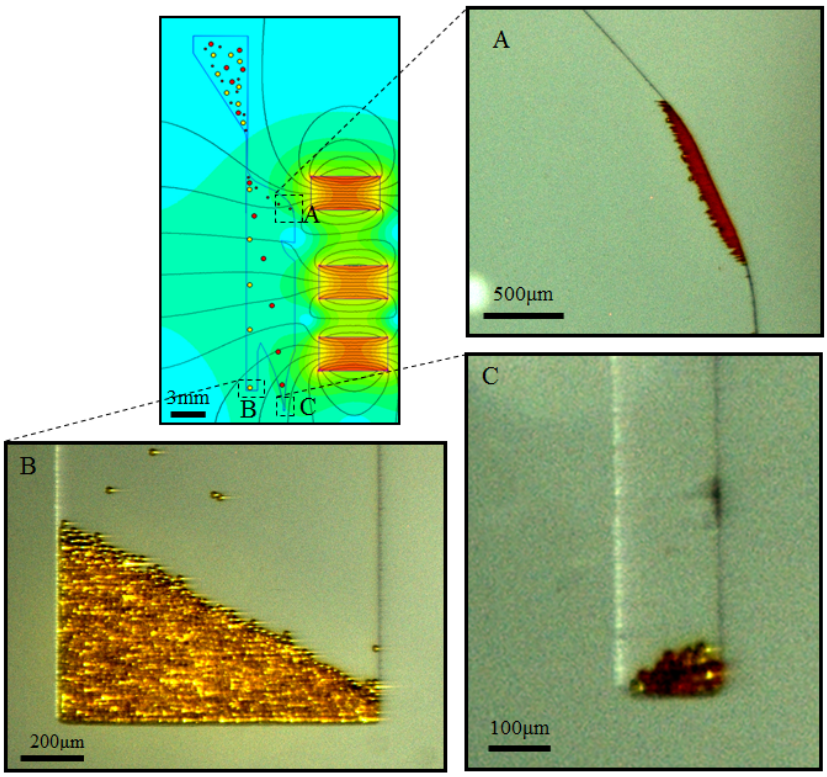

Figure 2.5: Results of biomimetic experiments with a large concentration of 20μm yellow non-magnetic beads and red 1μm magnetic beads representing healthy cells and tagging particles respectively and a very low concentration of red 20μm magnetic beads representing tagged cancer cells. The position of the images (taken from one of the 5 runs) is indicated on the schematic. The separation was done with a very high affinity, very close to 100%. Statistical results from the five runs can be seen in table 2.1 which indicates the average number of each particle captured in each area. Percentage values are also given. The fact that this level of separation can be achieved from a mixed population of three samples shows great promise for applying this system to separate cells in a blood sample.

ods such as blood separation through centrifugation [18, 21, 39, 41, 47, 48]. This suggests great opportunity towards a full-fledged, high-performance sample-to-answer system for a wide spectrum of applications involving a cell separation function.

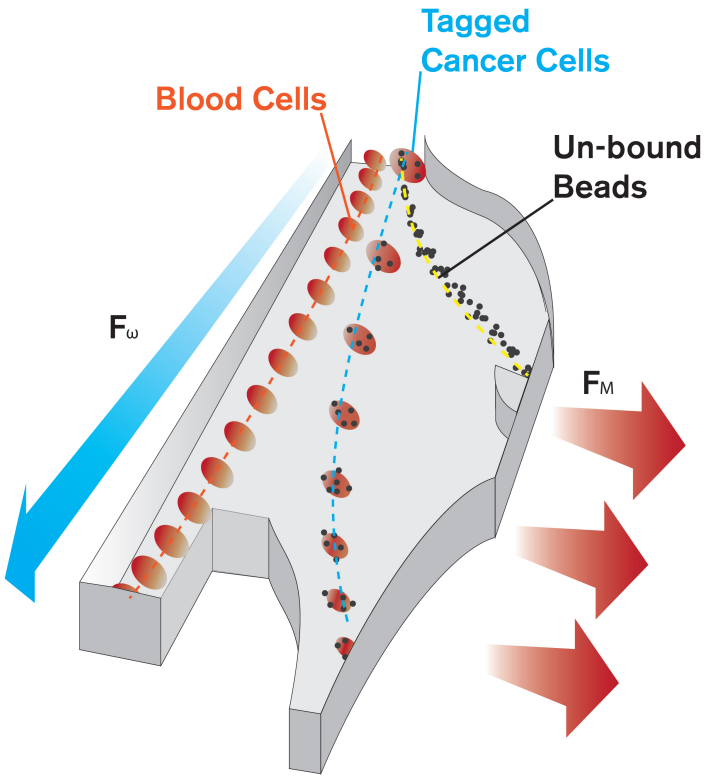

Figure 2.6: Schematic of the centrifugo-magnetic principle as applied to separating magnetically tagged cancer cells from a background of healthy blood cells and excess tagging beads. The principle is the same as the bead separation and shows great promise as a method of separating cells, for example CTCs from a background of healthy cells.

Chapter 3

Cell based on-disc magnetophoresis and enumeration

This chapter is based on the following publication:
Rapid and Cost-Efficient Enumeration of Rare Cancer Cells from Whole Blood by Low-Loss Centrifugo-Magnetophoretic Purification under Stopped-Flow Conditions,
Daniel Kirby, Macdara Glynn, Gregor Kijanka, Jens Ducrée,
Cytometry Part A 87.1 (2015): 74-80.

Following on from the results in chapter 2 where biomimetic "pseudo cells" were used to prove the principle of centrifugal magnetophoresis, the substantially improved design and functionality of the centrifugo-magnetophoretic platform which integrates direct immuno-separation and cost-efficient, bright-field detection of cancer cells in whole blood was developed. Like the earlier device, we aimed to contain all microfluidic and magnetic components on the convienient footprint of a common CD and the same centrifugal spin-stand instrument was used for rotation and visualisation of the disc. In a first step, target cells in a blood sample are specifically bound to paramagnetic microbeads. The sample is then placed into the disc cartridge and spun. In the second step, magnetically tagged target cells are separated by a co-rotating, essentially lateral magnetic field from the background population of abundant blood cells, and also from unbound magnetic beads. A stream of target cells centrifugally sediments through a stagnant liquid phase into a designated detection chamber. The continuous, multi-force immuno-separation proceeds very gently, i.e. the mechanical and hydrodynamic stress to the target cells is minimized to mitigate the risk of cell loss by collective entrapment in the background cells or vigorous snapping against a wall. We successfully demonstrate the extraction of MCF7 cancer cells at concentrations as low as 1 target cell per μl from a background of whole blood, with capture efficiencies of up to 88%. Its short time-to-answer is a notable characteristic of this system, with 10% of target cells collected in the first minute after their loading to the system, and the remainder captured within the following ten minutes. All of the above mentioned factors synergistically combine to leverage the development of a prospective low-cost point-of-care device for CTC detection.

3.1 Introduction

Over the past two decades interest in the centrifugal microfluidic lab-on-a-disc (LoaD) concept[18] has significantly increased, in particular for bioanalytical assays. The platform has been applied to successfully integrate liquid handling and detection for endpoints such as sample nucleic acid amplifica-

tion, immunoassays [49] and cell analysis [19, 40] The use of the inherent centrifugal field to transport and manipulate (liquid) analytes and reagents (rather than through complex actuation schemes such as pumps) makes the LoaD platforms particularly attractive for point-of-care (PoC) settings where both, cost-efficiency and robustness are prerequisites. Processing of the disposable disc-cartridge generally requires a speed-adjustable spindle motor as, for instance, found in conventional DVD players; indeed, such cartridges have previously been processed by the DVD-ROM drive of a laptop [50]. Additionally, the innate ability of centrifugal sedimentation makes LoaD platforms particularly suited to blood processing and cell handling. Very dynamically emerging trends of personalised medicine and acute healthcare have underpinned the need for advanced point-of-care (PoC) devices or companion diagnostics which can be deployed at the bedside in hospitals, in doctors offices and even at home for patient self-testing. Classically these tests have been carried out in central laboratories, involving long time-to-answer and high costs of instrumentation. Microfluidic platforms bear the promise to enhance patient comfort through fewer visits to clinics and more gentle blood sampling due to reduced volume requirements while alleviating the burden on health-care budgets. In addition to mobile monitoring of disease, these devices have also become a major driver of cell-based medical analysis in clinics and hospitals. A primary objective for such application is in the detection of extremely rare circulating tumour cells in whole blood samples. The field has considerably advanced in recent years, [51, 52] with a growing number of research groups investigating a range of aspects, from biological characteristics of cancer cells [53] such as the links between CTCs and metastases [54], to instrumentation designed for diagnostics based on counting the actual CTC numbers present in the blood [6], associated prognosis [55], methods of enumerating and detecting CTCs [51, 56, 57] and research into developing diagnostic devices which are able to detect CTCs in typical clinical settings [52]. Tools for CTC detection are expected to provide important, ideally patient-specific information for cancer prognosis, diagnosis, assessment of minimal residual disease and assessment of anti-cancer drugs [58]. Much effort is directed towards the development of microfluidic sys-

tems for detecting CTCs [59–63]. The paramount challenge is the extreme sparseness of such cells. While the CTC concentration in a patient sample is known to vary greatly with cancer type and stage [56], the scientific community has not yet been able to define a gold standard experiment for the unambiguous identification of a CTC; hence also a wide consensus on their concentration range is notably lacking. Nevertheless, we here follow the assumption of a concentration in the range of 1 cell per μl [6, 7]. However, note that some work refers to concentrations lower than 1 cell per ml [8], a concentration which would require an initial enrichment on our current system, for instance implementing RBC lysis or buffy coat extraction. Due to the extreme paucity of these cells, an efficient and reliable diagnostic instrument must meet particular performance criteria:

1. A capture platform must isolate the entire CTC population present (low loss, high capture efficiency).

2. It must discard background non-target cells (high isolation purity/specificity).

3. It must perform this analysis sufficiently fast.

4. It must handle rather large volumes of sample (high system throughput) [52].

CTCs have been distinguished based on size, deformability and density [64–66]. However, these physical parameters may significantly vary throughout the CTC population and thus also lead to significant overlap with normal cells. The majority of platforms, including the first commercially available CTC diagnostic system (Cellsearch, Veridex), therefore identifies CTCs based primarily on their specific protein marker expression such as epithelial cell adhesion molecule (EpCAM) via immuno-affinity binding [56] or immunomagnetic isolation [67–72]. In addition, negative markers, biophysical characteristics (e.g. size and deformability) and morphological analysis of CTC candidates are commonly employed. This chapter presents work on a novel centrifugal microfluidic system that can magnetically isolate, enumerate and detect rare cells on a low-complexity platform which is highly amenable to

PoC diagnostics. The previous chapter demonstrated continuous separation of magnetic beads of varying sizes from a large background of cell-mimicking beads but this chapter will describe the advancement of the earlier technology to isolate much lower, biologically relevant concentrations of cultured MCF7 breast cancer cells (from cell lines) spiked into a whole blood sample. We use paramagnetic, antibody-coated microbeads which target the MCF7 cells by binding to the EpCAM epitope expressed on these cells with very high specificity. Our continuous-mode, centrifugo-magnetophoretic system can therefore separate the input sample into its three superordinate constituents: (red and white) blood cells, magnetically tagged target (cancer) cells and excess unbound magnetic beads. A unique feature of this multi-force separation is the removal of unbound paramagnetic beads from tagged magnetic cells based upon the synergistic interplay of magnetic and centrifugal fields with the size-dependent Stokes drag. While many platforms [73] have used magnetic separation, they lack the ability to reliably separate unbound magnetic beads from isolated tagged target cells. This is because such a purification, e.g. through integrated size filtration, tends to be prone to clogging and unspecific trapping, and may thus lead to the loss of scarce target cells which would be prohibitive for rare cell detection. Our filter-less, flow-less sedimentation-driven system presented here, by design, eliminates this critical flaw. Through the continuous sedimentation scheme, we also mitigate the risk of cell damage due to vigorous snapping of beads against the vessel wall and the risk of collective pull of entrapped target cells by the abundant background population into the waste; these parasitic loss mechanisms are deemed prevalent in common batch-mode magnetostatic separations. Alongside presenting, for the first time, isolation of EpCAM positive cancer cells in biologically relevant concentrations using continuous centrifugo-magnetophoresis, we also demonstrate a proof-of-concept of a simple, bight-field method to quantitate the number of isolated cells based on their packing volume in the capture chamber. This technique is similar to established packed-cell-volume (PCV) haematocrit measure-ment [74] and is also being used on other diagnostics platforms [75].

3.1.1 Working Principle

In our stopped-flow, continuous sedimentation centrifugo-magnetophoresic device (Fig. 3.1), the three forces governing the path of the particles through the system, as discussed in detail in chapter 2, are the centrifugal force F_ω, the essentially lateral magnetic force F_m and the hydrodynamic Stokes drag F_D . Non-magnetic background blood cells will only experience the radial centrifugal force F_ω and the counteracting Stokes drag F_D to sediment on a straight path towards the peripheral edge of the disc. Concurrently, magnetic particles will additionally experience the lateral magnetic field F_m, and thus deflect from the main stream. The separation between unbound magnetic beads and the magnetically tagged cancer cells (Fig. 3.1c) is primarily governed by the differences of (the densities of) their magnetic momenta; the bulk magnetized beads possess a notably larger mean magnetic momentum than the much larger cell / bead hybrids which only exhibit a magnetization on the surface of their biological core. The resulting differential in lateral magnetic deflection is enhanced by the steep increase of field gradient towards the co-rotating magnet, which thus amplifies the spatial separation compared to a (hypothetical) uniform field and deflection of cells, akin to the "pseudo cell" deflection in chapter 2 is seen.

The two other factors, the centrifugal field and the viscous Stokes drag, are significantly smaller in magnitude and do not directly alter the deflection of the particle, i.e. the principal discriminator of our spatial separation technique. Instead, the interplay of these two counteracting forces mainly impacts the (radial) speed of sedimentation, which is only indirectly resolved by our technique through the residence time of the particles within the impact zone of magnetic deflection. However, the density differences between our types of bioparticles are significantly less pronounced than the differences in their magnetization, so the centrifugal field only constitutes a secondary effect in our separation mechanism. Our stopped-flow centrifugo-magnetophoresis therefore drives a central stream of copious background cells into the radially aligned, main waste chamber (labelled X in Fig. 3.1c). The most strongly magnetized, free beads are directed into a laterally aligned gutter chamber

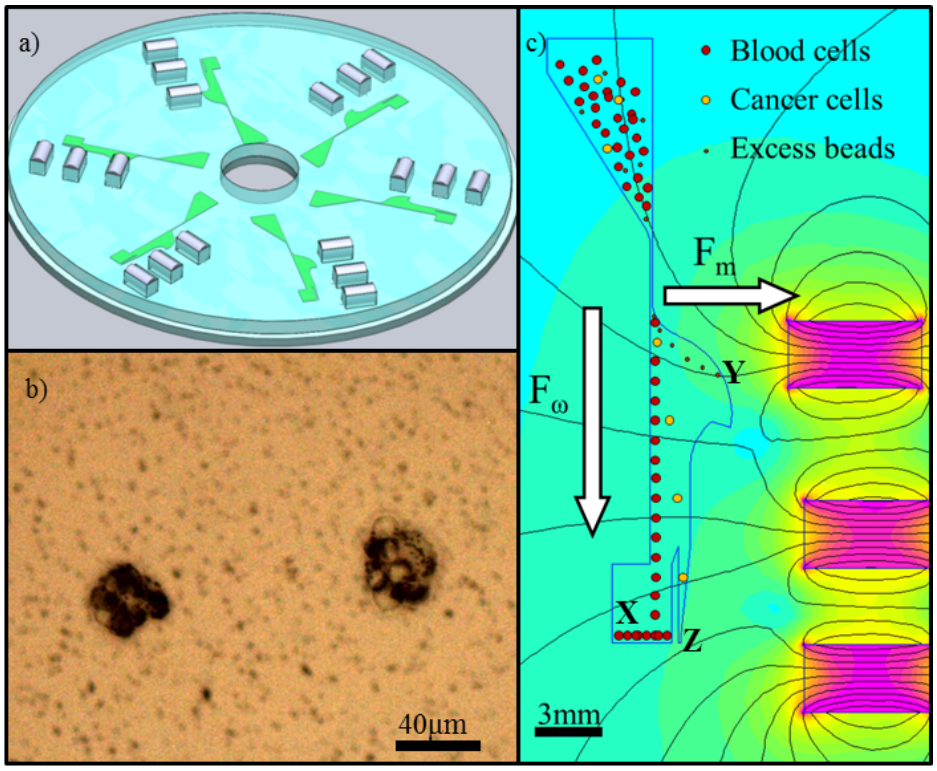

Figure 3.1: Schematic of the polymeric lab-on-a-disc with microfluidic channels, visible in green, and magnets as silver cylinders. b) Bright-field microscope image of two clusters of MCF7 cells tagged with paramagnetic beads (background beads are visible as dark specks). c) Magnetic field simulation of one of the green chambers from (a), with trajectories for blood cells, magnetically tagged (cancer) cells and excess magnetic beads. The directions of the centrifugal (F) and magnetic (Fm) fields are also indicated. Blood cells, excess beads and cancer cells are routed to the blood waste (X), bead waste (Y) and target cell capture chamber (Z), respectively. Direction of rotation is CCW.

(labelled Y in Fig. 3.1c) due to the balance of drag, magnetic and centrifugal forces discussed in chapter 2.3.1. Finally, the less magnetised hybrids of the target cells with the bead-tags are routed closer to the main sedimentation direction into a slightly displaced, small detection chamber (labelled Z in Fig. 3.1c). Direction of rotation is counter-clockwise (CCW), which means any corialis effects will keep particles against the left-hand wall (Fig. 3.1c). Due to the low speed of sedimentation of the particles in stopped-flow mode,

the impact of the Coriolis force was found to be negligible, but the sense of spinning direction was chosen as a precaution anyway. In this way our design provides a low-stress, three-fold spatial separation of background blood cells, magnetically tagged cancer cells and excess tagging beads. Compared to standard, batch-mode immunomagnetic separation with a simple magnet, our continuous, sedimentation-driven system separates the latter two magnetic particles without the error-prone size filtration. Furthermore, the novel, stopped-flow mode inherently eliminates flow-field instabilities which tend to compromise resolution. Also, magnetostatic, batch-mode immunoseparation often leads to collective entrapment of rare target cells in a cohort of background cells. This loss mechanism is suppressed through the radially stretched distribution of the population of suspended cells through the continuous sedimentation mode.

3.2 Materials and Methods

3.2.1 Disc Manufacture

The manufacture of the microfluidic discs was almost identical to the process in chapter 2. But, in brief, the discs were formed from polydimethylsiloxane (PDMS) (Sylgard 184, Dow Corning; #101697, Farnell, UK) by standard soft lithography methods from a design drawn with AutoCAD (Autodesk, Inc., CA, USA). A 100-μm thick dry-film photoresist (DuPont, NC, USA) was hot-roll laminated onto a 4 inch silicon wafer, lithographically structured by UV exposure and developed according to the manu-facturers instructions. The dry film structures left on the wafer define the PDMS casted channels. The millimetre-scale indentations for magnet positioning (Fig. 3.1 a) were engineered with a 3D-printed polymer mould (uPrint, Stratasys Ltd., MN, USA) and aligned via guide pins to create highly reproducible discs with both, micro- and macro-features. After the PDMS had been poured into the mould and hardened in the oven (1 hr at 70°C), the discs were assembled and then placed for one hour into a vacuum chamber to allow subsequent, degas-driven priming [44] with buffer (Phosphate buffered saline [PBS] with 10%

EDTA and 1% casein). The magnets (S-03-06-N, Supermagnete, Germany) were then placed into the pre-moulded voids on the PDMS disc.

3.2.2 The centrifugal spin-stand

The microfluidic disc is then loaded with sample and placed onto the same custom designed centrifugal spin-stand as chapter 2, featuring a servo motor (4490 series, Faulhaber, DE), a CCD camera (Sensicam series, PCO, DE) connected to an optical imaging system (Navitar, NY, USA) and a strobe light all synchronised via a PC (DELL, USA). The system records one image per rotation, giving the user a live feed of the cells and microparticles as they sedimented through the microfluidic chambers. This provided detailed trajectory information and real-time counting of target cells, even during high-speed rotation.

3.2.3 Bead and cell binding

The basic separation mechanism here presented is dependent on specific binding of the 4.5μm diameter magnetic microbeads to the target cells of interest (Fig. 3.1 b) (Dynabeads Epithelial Enrich, Invitrogen Inc.). The Dynabeads were diluted 80-fold from stock and incubated at a 1:1 volume ratio with MCF7 cells spiked. All culture reagents were obtained from Sigma-Aldrich (MO, USA) unless otherwise stated. MCF7 cells (DSMZ, Braunschweig, Germany) were cultured in 75cm^3 flasks in DMEM media, supplemented with 10% uninactivated foetal bovine serum (FBS), 100 U/ml penicillin and 100μg / ml streptomycin. Cultures were maintained at 37°C with 5% CO2. Cells were harvested by incubation in 5ml 0.25% trypsin / 0.1% EDTA at 37°C for 5 minutes followed by neutralization with 5ml culture medium. Cells were centrifuged at 300g for 4 minutes and resuspended in culture medium. Where indicated, live cells were fluorescently labelled with NucBlue Live Cell Stain (Life Technologies, CA, USA) according to manufactures instructions. Whole blood, MCF7 cells and Dynabeads were incubated in a capped 2ml tube on a rotator for approx. 10 minutes at room temperature. It was noted

that substantial MCF7-cell-to-bead binding was observed within less than 5 minutes.

3.3 Experimental Results

3.3.1 Centrifugo-magnetophoresis

Following incubation of the sample with magnetic beads, a 3μl aliquot was loaded into each of the six chambers of the prepared microfluidic disc, providing a total volume of 18μl. This sample of whole blood, tagged MCF7 cells and excess beads was then sedimented through the system by rotating the disc at a rate of 17Hz (55g at edge of disc). When viewed using a magnified real-time video stream of the microfluidic chambers, within 10 seconds the first of the tagged MCF7 cells can be seen to exit the focusing channel (Fig. 3.2) and are then deflected by the magnetic field into the designated capture chamber. Within 1 minute the first MCF7 target cells are routed to their designated capture area. The remainder of the particles (untargeted red and white blood cells, beads and the remaining tagged cells) continue to sediment down the chamber to their respective capture areas (Fig. 3.1c); within 10 minutes the separation is completed.

As shown in Fig. 3.3 and described in chapter 3.3.2, the centrifugo-magnetic stopped-flow system very accurately and reproducibly separates a very small number of target cancer cells from a background of a whole blood down to concentrations as low as 1 cell per μl. Furthermore, the system can also very efficiently segregate the unbound background beads without error-prone steps such as size filtration. This removal of the unbound beads is of critical importance for the quantification of the captured cells, as, otherwise, their presence in the target chamber would influence the level of packing measured.

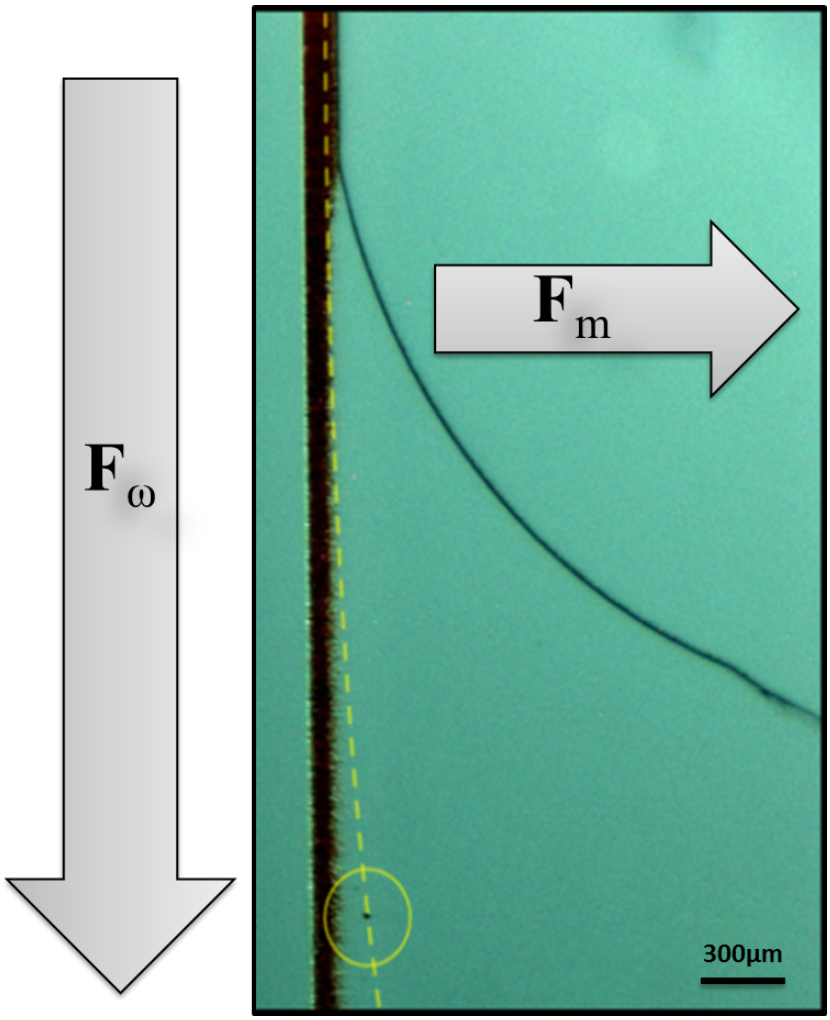

Figure 3.2: Image obtained of bulk blood cells travelling radially outward while a magnetically tagged cancer cell is additionally deflected by a laterally placed magnet. The yellow line shows the path taken by the tagged cancer cell which is circled in yellow. Image is taken at the enterance to the separation chamber (See Fig. 3.1 c)

3.3.2 Detection and quantification

In order to engineer a low-cost and easy to use system, we obviated the need for any complex procedure and costly fluorescence imaging. Unlike many other published instrumentation [60, 63] the specificity of detection in our system is not based on the binding of a specific fluorescent antibody, but rather on the specificity of the magnetic beads to the target cells of interest.

As these cells are isolated from the background sample, and specifically directed to a dedicated detection locus, our here presented detection technique is based simply on analysing the extent of occupation of this locus using bright-field imaging (Fig. 3.3a).

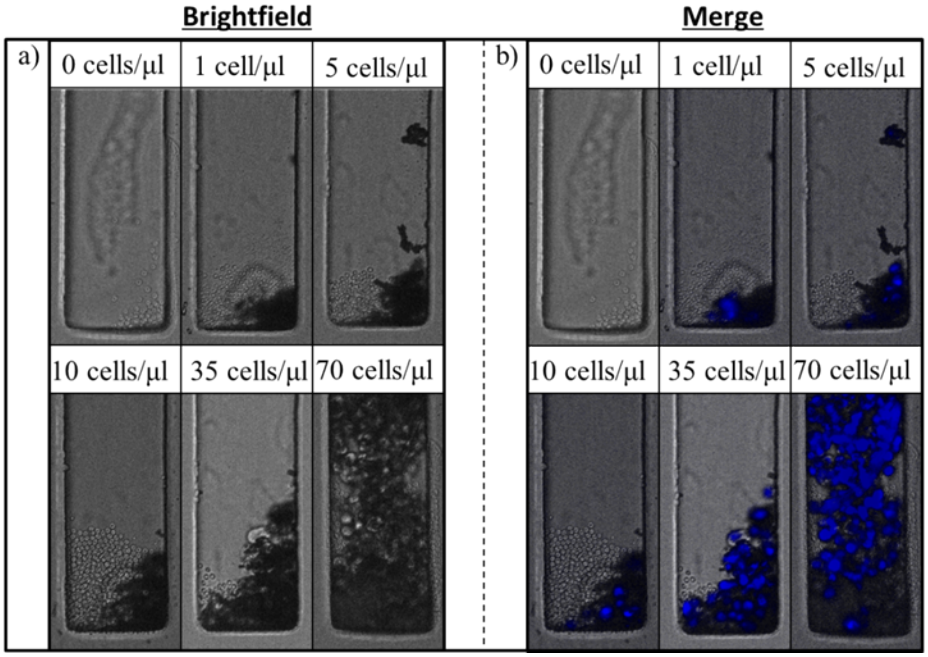

Figure 3.3: a) Bright-field image showing the magnetically tagged MCF7 cells in the capture chamber. This method was used for counting the dark pixels (tagged MCF7s) with the freeware ImageJ (See Fig. 3.4). b) Fluorescent merge image displaying the same magnetically tagged and NucBlue stained MCF7 cells in the capture chamber. This method was used to enumerate the amount of MCF7 cells present in the entire system, including any cells which did not reach the capture chamber in order to calibrate the system. Chamber width: 150μm

The dark areas shown represent clusters of target cells surrounded with magnetic beads which are tightly packed by the centrifugal field. The darkness of the filling arises from the bead tags, and this facilitates simple image processing to quantify the extent of packing. The surface area of the pack was found to be directly proportional to the (pre-defined) concentration of tagged cells in our spiked sample (Fig. 3.4). In order to quantify the exact number present for calibration purposes we fluorescently labelled the MCF7

cells with NucBlue dye beforehand (Fig. 3.3b). Note that for the later analysis and quantification, only the bright-field images were used.

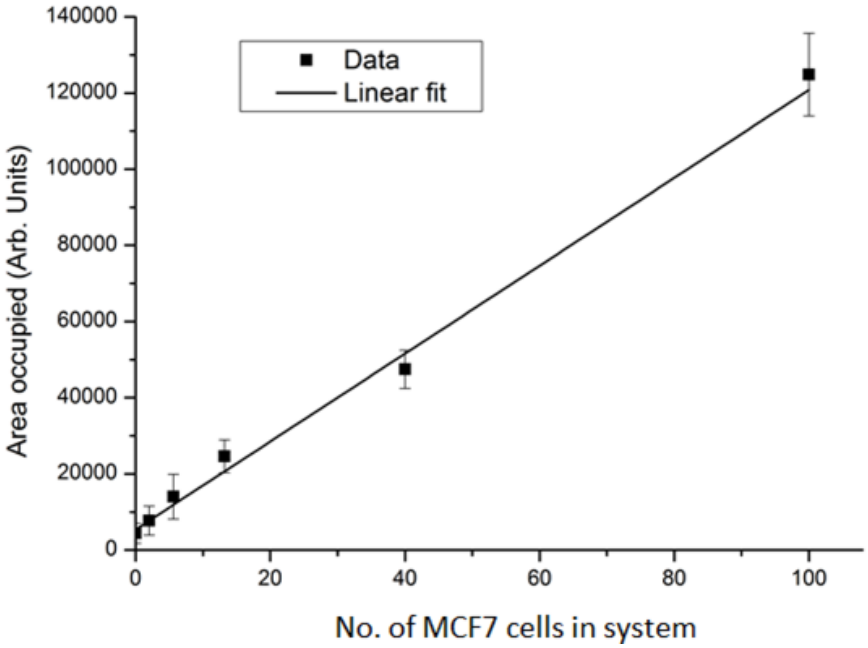

Figure 3.4: The area of the capture chamber occupied by dark pixels was calculated on ImageJ software and plotted against the total number (determined by fluorescent tagging) of MCF7 cells in the sample, giving a very close linear fit ($R^2 = 0.98$ and $n = 5$). This standard curve gives a baseline calibration to determine the concentrations of target cells present based on determination of the dark area.

We analysed the bright-field images of the target cell capture chambers of all structures on the disc. Due to the high contrast of the cell / bead pack with respect to the background in the capture chambers, a straight-forward method as part of the freeware image analysis software ImageJ (ImageJ, U.S. National Institutes of Health, MD, USA) could be employed to enumerate the number of dark pixels in a pre-defined region of interest, and thus measure the extent of packing within each sample. In brief, the background signal defined a threshold value and the image was converted to an 8-bit binary picture. The histogram could then be adjusted to provide the maximum contrast between the dark bead / cell clusters and the bright background.

This gave a clear count of only the black pixels and widely suppressed noise from untagged blood cells or other stray particles. A set of six discs, with each running five identical samples, was analysed using this method.

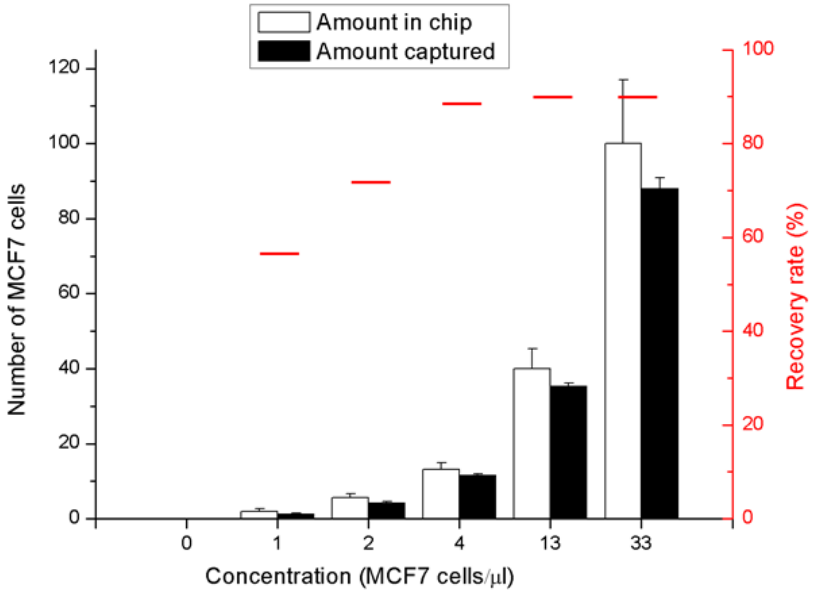

Figure 3.5: The total amount of MCF7 cells present in the chip is indicated in white, while the total number captured successfully is indicated in black. The mean recovery rate (indicated in red) is 80% (n = 5), peaking at 88% at the highest concentration.

The total amount of MCF7 cells present in each of the whole blood tests, and the corresponding area calculated by the dark packing fraction method are shown in Fig. 3.4. The correlation between packing area and known input is demonstrated by the standard curve of the graph. These estimated values correlated directly with the actual values shown in Fig. 3.5, while the analysis strategy successfully identified the healthy sample (i.e. zero cancer cells) and also correctly assigned the values to the increasing concentrations of cancer-cell spiked samples that were as low as a single MCF7 cell per μl of whole blood sample. The capture efficiency, i.e. the ratio between the number of cancer cells retrieved after centrifugo-magnetic purification vs the

total number of cancer cells introduced into the chip, is 80% on average, peaking at 88% for the highest concentration (Fig. 3.5).

3.4 Conclusions and outlook

We have presented the centrifugo-magnetophoretic purification and bright-field based quantification of rare cells from whole blood. A test on 3μl of sample in each chamber rapidly completes within ten minutes on our lab-on-a-disc system; the first target cells are even detected in less than one minute, which might be beneficial if the sheer presence of the diagnostic target cell was relevant (e.g. in the case of circulating tumour cells). The mean recovery ratio of the target cells was 80%, peaking at 88% towards higher concentrations. The target cell population can be quantified by a low-cost, bight-field opto-mechanical setup incorporating a spindle motor and a CCD-based readout akin to an optical disc drive like a CD or DVD player. We also note that this system could detect cells at a much lower concentration than here presented if the sample was purified and concentrated prior to the centrifugo-magnetophoretic procedure, e.g. by band extraction of the buffy coat or lysis of the erythrocytes. It is also worth noting that while EpCAM was used in these particular experiments, any target (or combination of targets) can be used through adoption of widely recognized bead technologies and bead-binding chemistries. Our system may thus be readily advanced to a compact, rapid, accurate and fully automated sample-to-answer (rare) cell counter for point-of-care diagnostics.

Chapter 4

Centrifugal Diamagnetophoresis

4.1 Preamble

As the research into detection of CTC's advanced, it became clear that it was important to develop technologies that were not only based on positive epitope expression, as not all CTC's could be found in that fashion. Size based and negative selective methods were also seen to be of importance when developing a device capable of detecting CTC's [76, 77]. As a side-project to the original research track, it was envisaged to try to adapt the centrifugal microfluidic platform to perform negative magnetophoresis. That is, magnetically removing all the healthy blood cells and leaving behind all the cells which did *not* express the well known white blood cell surface markers CD45 and CD15 and thereby isolating possible CTC's based on their absence of a specific marker. This work was published by Glynn *et al.* [78] with experimental assistance by the author. Subsequent investigation into negative selection methods by the author led to the next section of this work, a method of label free, size and density based separation of pseudo cells by centrifugal *dia*magnetophoresis which is outlined in this chapter.

4.2 Introduction

In order to expand the scope of the centrifugal magnetophoretic stopped-flow platform to enable label-free, size and density based separation of cells it was necessary to think about alternate methods of separating candidate CTC's from a blood background. As opposed to the negative magnetophoresis explored by Glynn *et al.* and the paramagnetic deflection discussed in chapters 1-3, it was proposed that, with a very similar set-up as before, it would be possible to exploit the centrifugal magnetophoretic platform to enable diamagnetic deflection of particles AWAY from a magnet, if the particles were suspended in a paramagnetic liquid. This method had many advantages and was explored as a possible label free sorting technique for cells based on either a mass, size or density difference. These property differences would in turn effect the magnetic deflection force AWAY from the magnets and the centrifugal force, thus resulting in diversion of particles to different capture chambers depending on their properties. Another advantage was the fact that a particle attracted towards a magnet will feel a rapidly increasing magnetic force (with a r^3 relationship) that can easily cause a particle to be very rapidly snapped towards the magnet and trapped. However, a particle being pushed away from the magnet will not suffer this effect and will undergo a much gentler deflection.

4.3 Theory

Most materials fall into the three main categories of magnetism. They are either paramagnetic, ferromagnetic or diamagnetic. A typical permanent magnet is ferromagnetic, a piece of iron which can be magnetised when in the presence of an external magnetic field is paramagnetic and most materials thought of as "non-magnetic" are in fact slightly repelled by a magnetic field. These last class of materials are "diamagnetic".

There are of course many sub categories and exceptions to this rough categorisation, but it is not necessary to go into any more detail for the scope of this work.

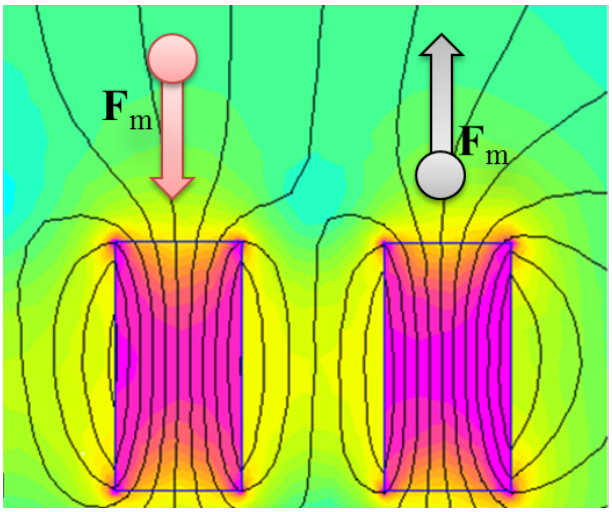

Figure 4.1: Magnetic field simulation (FEMM, USA). When in the presence of a magnetic field, a paramagnetic particle will be attracted towards the magnetic field maximum (left). Whereas, a diamagnetic particle will be pushed away from the magnetic maximum (right). This force is greatly increased if the diamagnetic particle is suspended in a paramagnetic liquid.

4.3.1 Pseudo cells

As in previous chapters, polymer beads were used to simulate various properties of cells to prove the principle before moving on to true biological samples. The pseudo cells in this case were 10μm polymer beads of varying densities, full details of which are given in the materials and methods section of this chapter. If a separation could be carried out based on slight density variations of beads, it was hypothesised that blood cells and cancer cells could be deflected to different regions on the disc as before, but in a label free fashion, purely based on density.

4.4 CTC detection

It has been shown that CTC's can be identified based on their slight size and density differences compared to normal blood cells [76, 79]. According to the work of Liang *et al.* the diagmagnetic force increases with the diameter of the particle suspended in a paramagnetic medium [80]. The sedimenta-

tion velocity of a particle will also be affected by particle size and density, as outlined in chapter 2.3.1. To this end it should then be possible to sort cells based on their size and density and therefore to identify CTC candidates in a label free fashion. While diamagnetic deflection of particles had been undertaken before [80], it was believed that the unique properties of the stopped-flow centrifugal system could offer a more accurate and less fluidically complex system that would enable subtle differences in size, density and shape of the target cells to be identified. In order to investigate the viability of a centrifugal-microfluidic diagmagnetic deflection system, a series of experiments were carried out on various different paramagnetic mediums and particles of varying size, mass and density.

4.5 Materials and methods

4.5.1 Disc manufacture

Discs were manufactured through the standard soft lithography technique used throughout the previous chapters. The main difference between this design was the location of the magnets on the opposite side of the separation chamber and the creation of the 10 finger structures at the end of the chamber to enable the final location of the beads to be accurately determined. The full disc schematic can be seen in figure 4.1 and a detailed view of an individual chamber can be seen in figure 4.2.

Once the discs had been prepared for degas flow as outlined in chapter 2, they were primed with the paramagnetic medium. This was either a water based ferrofluid (Liquids Research, UK #MJ300) or the paramagnetic salt, Manganese chloride($MnCl_2$) (Sigma Aldrich, USA). The ferrofluid was diluted at a ratio of 1:10 with a buffer of Phosphate buffered saline with 5% w/v of Bovine serum albumin and vortexed for 5 seconds. This made the ferrofluid light enough to be visualised through standard microscopy after the tests were performed while maintaining a high enough magnetic susceptibility to enable significant deflection of the diamagnetic particles. The paramagnetic salt was made up to a concentration of 1mM

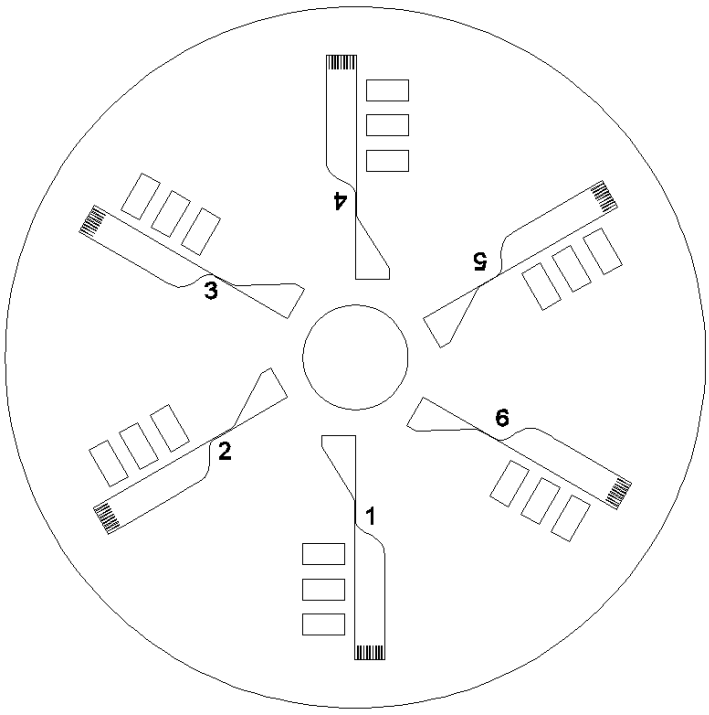

Figure 4.2: A PDMS disk of the same size as those used in all previous chapter was made with 6 identical chambers that had magnets located on the opposite side of the chambers as before. This was to implement the diamagnetic pushing force on the particles entering the chambers. Full details can be seen in Fig. 4.2.

in a buffer of Phosphate buffered saline with 5% w/v of Bovine serum albumin and sonicated for 5 minutes before vortexing for 30 seconds to ensure the salt had fully dissolved into the buffer. The three types of beads used were polystyrene (Microparticles GmbH, DE. #PS-FB-B1407 $\rho = 1.05 g/cm^3$ d=9.55μm), Polymethyl methacrylate (PMMA)(Microparticles GmbH, DE. #PMMA-R-B1073 $\rho = 1.19 g/cm^3$ d=9.57μm) and melamine resin (MF) (Microparticles GmbH, DE. #MF-FITC-L824 $\rho = 1.51 g/cm^3$ d=10.60μm).

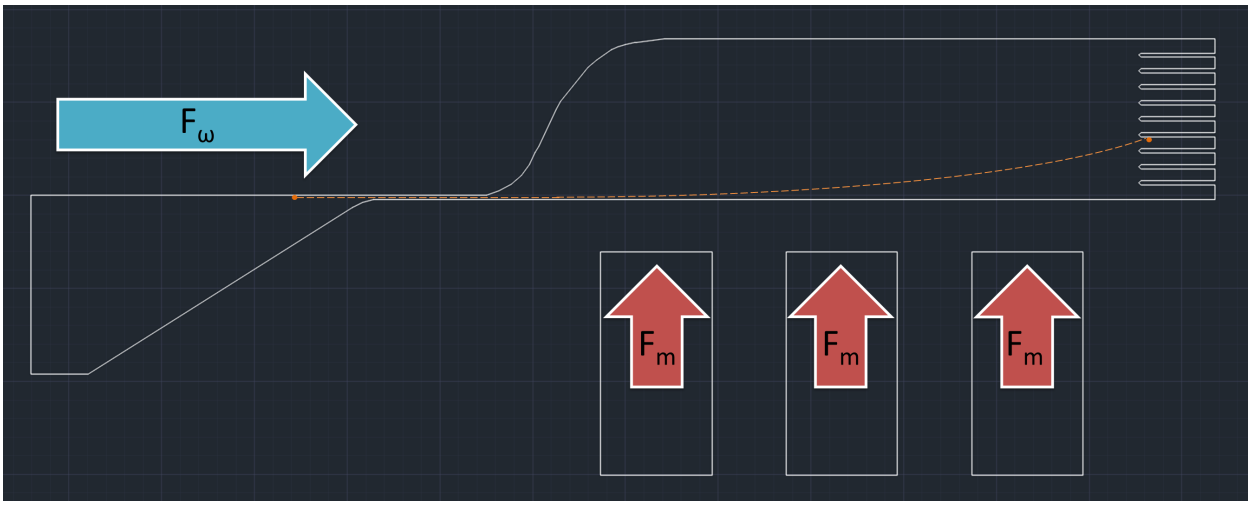

Figure 4.3: Diamagnetic deflection on the centrifugal platform. As diamagnetic particles were sedemented through a paramagnetic medium by the centrifugal force, they were deflected laterally AWAY from the magnets and into one of the ten capture "fingers". And example of a particle trajectory can be seen in orange.

4.6 Results

Once the discs were primed with the chosen paramagnetic liquid, a suspension of beads was loaded onto the disc. As in the previous chapters, 3μl of sample was loaded into each chamber. Each sample was spun at a frequency of 17.5hz and the results for each bead in the prepared ferrofluid are outlined below.

The final location of the three types of polymer beads are outlined below in Fig. 4.4 and the relevant capture statistics for each are given in the following three figures. Take note of the numbering system for each finger to compare the capture statistics to the schematic in Fig. 4.4.

After successful enumeration of the capture efficiency of the beads in the ferrofluid, it was important to prove the principle in the paramagnetic salt, as if the system was to move onto using biological samples the ferrofluid would not be a viable option, being toxic to cells. While due to time constraints it was not possible to perform the paramagnetic salt experiments to the same level of completion as done for the ferrofluid, the concept was proven and

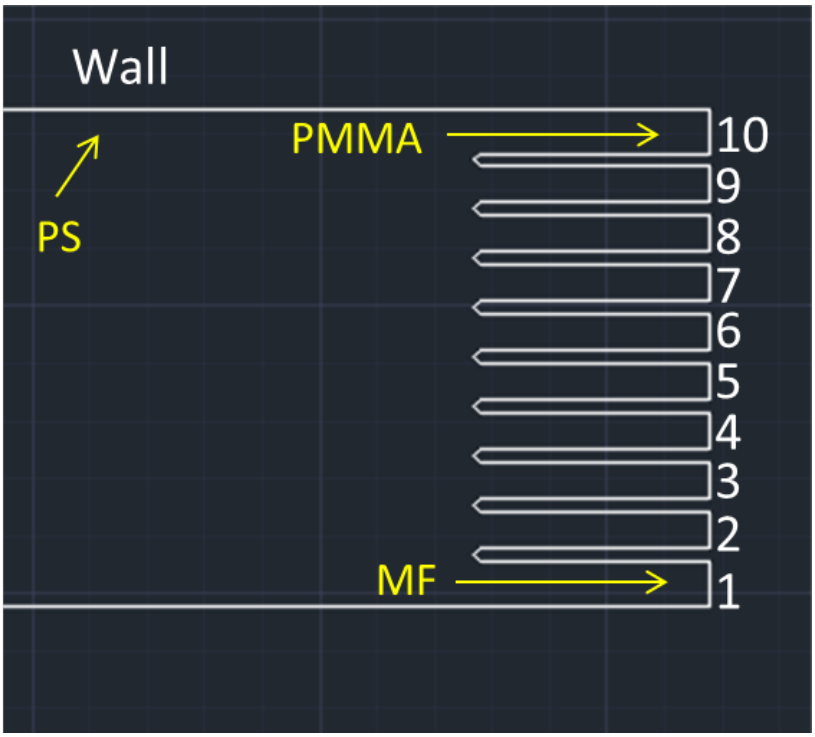

Figure 4.4: The final location of the majority of each bead type is indicated above. The most dense particles (MF) were located in finger 1, having undergone very little deflection. The medium density particles (PMMA) were located in finger 10, furthest from the magnet, having undergone a significant deflection. The lowest density particles (PS) were mostly located against the chamber wall, having undergone a very large deflection and remaining pinned against the wall by the magnetic force.

deflection of polymer beads in the $MnCl_2$ liquid can be seen below in figure 4.8.

4.7 Conclusions and Outlook

It was shown in this work that it is possible to use the centrifugal magnetophoretic platform to separate with a very high accuracy, polymer microparticles with slight variations in density. And furthermore, this separation is carried out by a diamagnetic deflection, away from the magnet. This gentle pushing force is of great interest for implementation on a biological sample

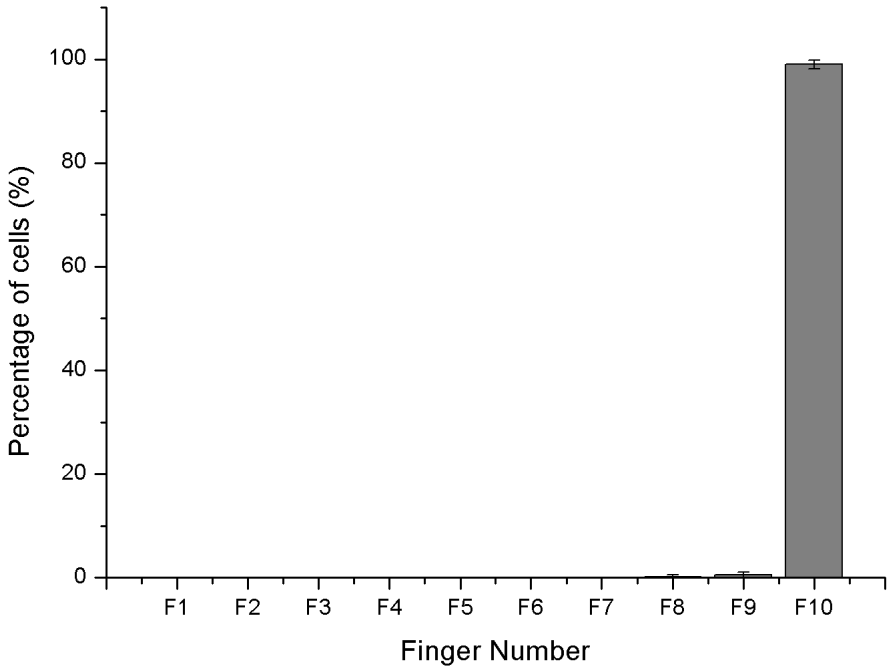

Figure 4.5: Final location of PMMA beads after deflection in 0.1x ferrofluid. Over 99% of the beads were located in finger 10, furthest away from the magnet. N=6

such as spiked cancer cells in whole blood, to laterally separate and hence detect any cells which vary in density with those of normal healthy blood cells.

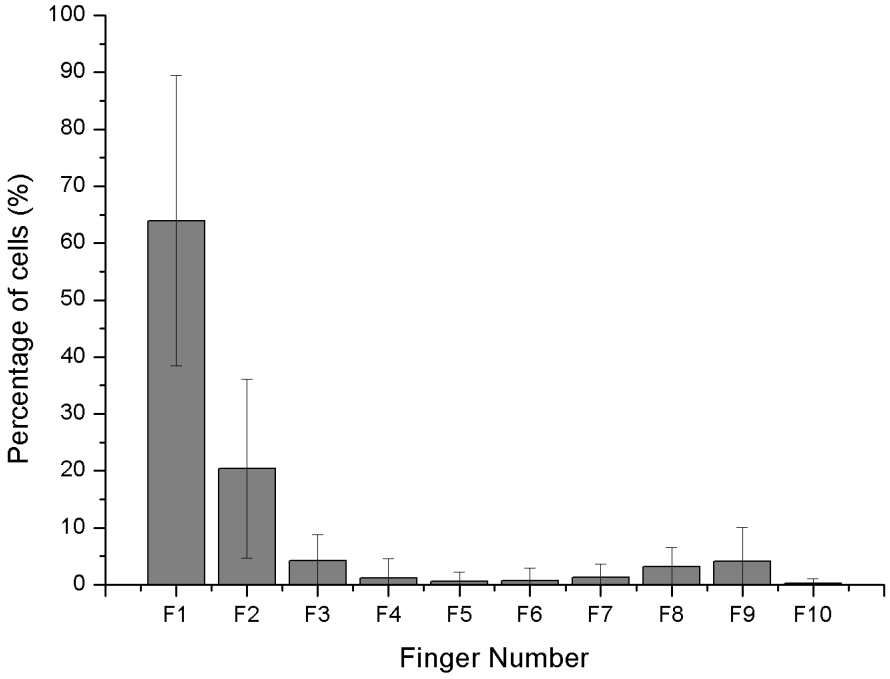

Figure 4.6: Final location of MF beads (highest density) after deflection in 0.1x ferrofluid. Over 60% of the beads were located in finger 1, with a small spread across the rest of the fingers N=6.

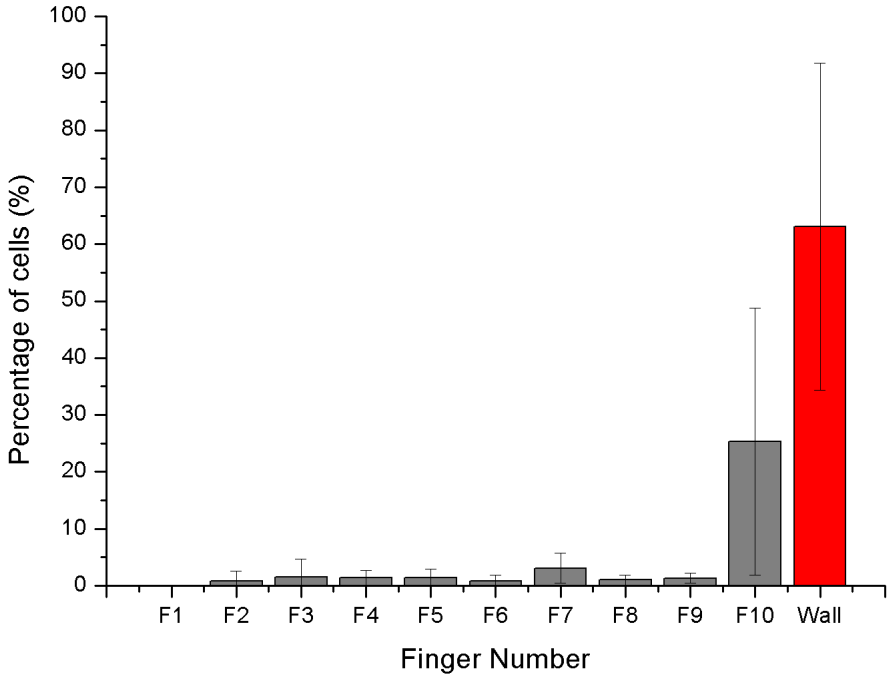

Figure 4.7: Final location of PS beads (lowest density) after deflection in 0.1x ferrofluid. Over 60% of the beads were located against the chamber wall furthest away from the magnets (seen in red) this is due to the increased lateral displacement vector keeping them pinned against the wall. N=6

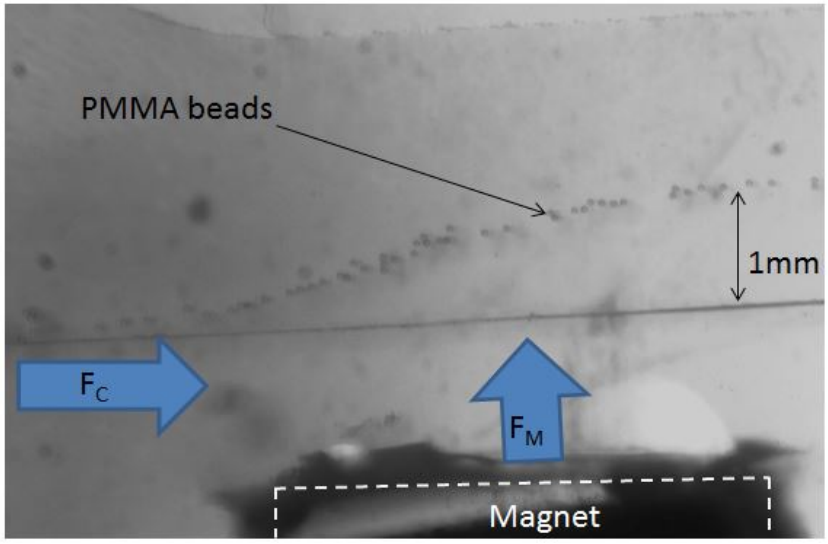

Figure 4.8: Diamagnetic beads in a paramagnetic medium being deflected AWAY from a magnet.

Chapter 5

Application of the Centrifugal Magnetophoretic Platform for HIV/AIDS Diagnosis

This findings in this chapter have been published as:
Centrifugo-magnetophoretic purification of CD4+ cells from whole blood toward future HIV/AIDS point-of-care applications,
Macdara Glynn, Daniel Kirby, Danielle Chung, David J. Kinahan, Gregor Kijanka and Jens Ducrée,
Journal of Laboratory Automation **19** (2013) 285-296.

The technology that was developed in chapters 2-4 for circulating tumour cell detection was also seen to show promise for many other applications, and a HIV/AIDS diagnostic was developed. The experimental work was conducted in tandem with Macdara Glynn. Glynn was the main author on the publication and a more thorough explanation of the work can be found therein. The concept was almost identical to the previous chapter, however it has been included to highlight the fact that the centrifugal magnetophoretic platform can be easily modified to fit a host of biomedical applications and is here shown to perform an actual diagnostic test for HIV/AIDS without need of sample enrichment. This is an example of centrifugal magnetophoresis being used for abundant cell capture, as opposed to rare cell capture.

5.1 Introduction

HIV/AIDS diagnostics are of particular importance in resource-poor regions such as Sub-Saharan Africa where as well as rates of infection being amongst the highest in the world, access to modern laboratories and medical care are not widespread. Point of care tests have been shown to be vitally important in this setting to increase chances of survival and quality of life [81, 82]. Many point-of-care devices have been developed for this very purpose and it is a currently expanding field with new products being conceived and coming to market since 2009. An extensive review of the field has recently been published [83].

This chapter will offer a brief overview of the use of the system for a HIV/AIDS diagnostic, but the full details can be found in Glynn *et al.*'s publication [84].

5.1.1 HIV/AIDS

The human immunodeficiency virus (HIV) and acquired immune deficiency syndrome (AIDS) are diseases of great concern worldwide and especially in Sub-Saharan Africa. The standard method of testing for HIV/AIDS is to count the concentration of a subsection of white blood cells in a patient blood

sample. These cells are called T-helper cells, but are often refered to as "CD4 cells" due to the CD4 epitope on their surface. In a healthy patient, these CD4 cells will be present at a rate of about 1000/μl,in a HIV positive patient the concentration will have fallen to about 500/μl whereas a patient with full-blown AIDS will have a concentration of less than 200/μl. The world health organisation have recommended that any patient with a CD4 count of less than 350/μl should immediately commence antiretoviral therapy to prevent HIV developing into AIDS [85]. Compared to the search for CTC's in blood (<1CTC/μl), these parameters were significantly easier to satisfy and offered an easily transferable use for the centrifugal-magnetophoretic platform.

5.2 Working Principle

The working principle is almost identical to the CTC diagnostic in chapter three, with two main differences. The target epitope on the cells of interest is different and the target cells are far more abundant than CTC's. This meant a change in magnetic beads to Dynabeads CD4 4.5μm magnetic beads (Life Technologies) so that the new target epitope could be bound.

Blood was extracted directly from healthy donors via finger prick using 1.5 mm sterile lancets (BD Biosciences, Franklin Lakes, NJ) and was then spiked with cultured CD4 cells at increasing concentrations in the medically relevant regime.

5.3 Results

The system easily differentiated between a blood sample spiked with CD4 positive cells and CD4 negative cells, with 92% of the CD4+ cells being directed to the capture chamber and only 0.6% of the CD4- cells being directed to the capture chamber. This enabled levels of CD4+ cells in the sample to easily be determined.

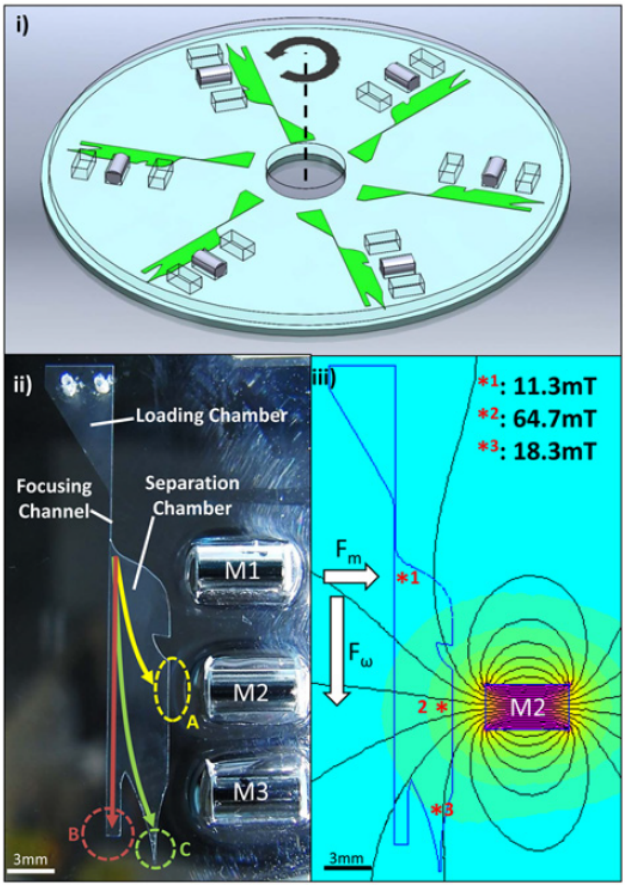

Figure 5.1: i) Schematic of the lab on a disc platform which is almost identical to that used in previous chapters. The magnet positioning has been adjusted to the optimal positioning for CD4 bead and cell capture. ii) Photograph of the capture chamber. Only the centre magnet (M2) was used during experiments. iii) A magnetic simulation giving the approximate field strength at various positions in the separation chamber was carried out for the new magnet configuration (Finite Element Method Magnetics (FEMM) 2010.

5.4 Conclusion and Outlook

If this technology were combined with the cell counting technique used in chapter 3 then a quantitative cell count could be performed to determine the concentration of CD4+ cells blood and hence deliver an actual HIV/AIDS diagnostic. This was the intended follow-on from this work and ultimately led to the development of a hand-held CD4 chip by Glynn *et al.* [86]. This

work all originated from the first inception of the centrifugal-magnetophoretic platform and is an excellent example of the many possible applications of this technology.

Chapter 6

Large Volume Blood Handling

The previous chapters have only worked with volumes far too low to ever be of any clinical significance (3μl per chamber) for a CTC detection device [7, 8, 77]. This chapter discusses the necessary steps taken and the results obtained after the move from handling approximately 3μl of sample on the magnetophoretic cell separation platform to handling 0.2ml of sample. The limit of detection was also improved upon as compared to chapter 3, where 1 cell/μl was the limit, to a limit here of 0.1 cells/μl. This almost two order of magnitude increase in sample volume along with a one order of magnitude improvement in the limit of detection allowed the device to move from a basic proof of principle platform towards becoming a viable method of finding real CTC's in a patient sample.

6.1 Introduction

In order to load a blood sample of sufficient volume to enable clinically relevant amounts of blood to be analysed, it was envisaged that a loading structure that was located at the centre of the disk which would simultaneously sediment the sample through all 6 microfluidic chambers at once would offer the best chance of high-volume throughput (Fig. 6.1).

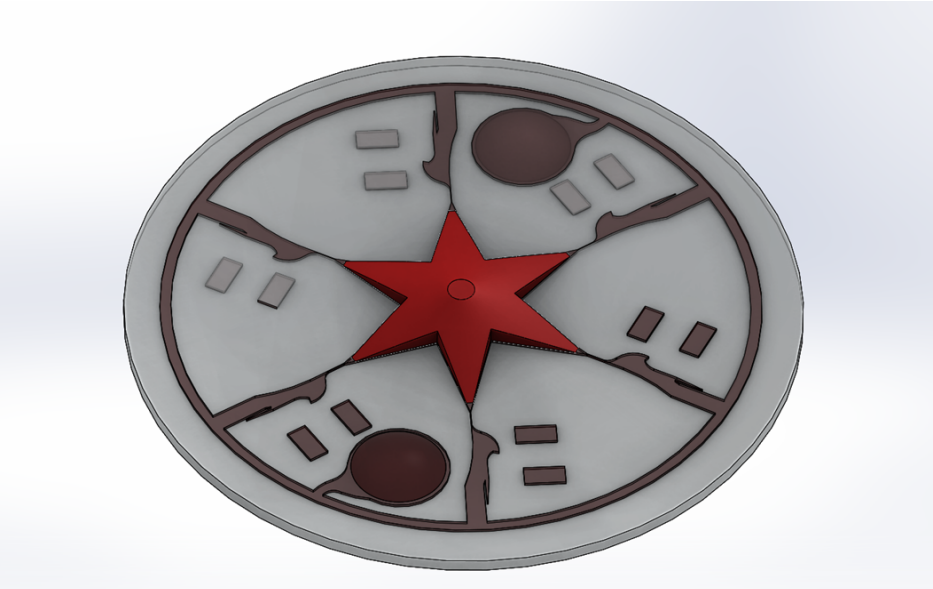

Figure 6.1: Schematic of the high volume design with the 3D printed centre mould (red) enabling multiplexing of the large volume blood sample through all six chambers simultaneously. Disc diameter=100mm

The unique benefits of centrifugal microfluidics were once again made apparent as the centrifugal force, acting from the disc centre would simultaneously sediment any particles outwards in all directions (Fig. 6.2).

6.2 Materials and Methods

6.2.1 Disc Design

The disc designs mentioned in chapters 2 and 3 were never going to be able to detect a CTC at a realistic concentration [7] because of the volume constraints present due to the loading chamber size and manufacturing techniques used (photolithography). It was necessary to completely redesign the disc using a multitude of manufacturing methods in order to achieve the necessary macro to microfluidic stopped-flow network. This was done through a combination of photolithography, 3D printing and both red and clear PDMS casting resulting in the final design, seen in figure 6.1.

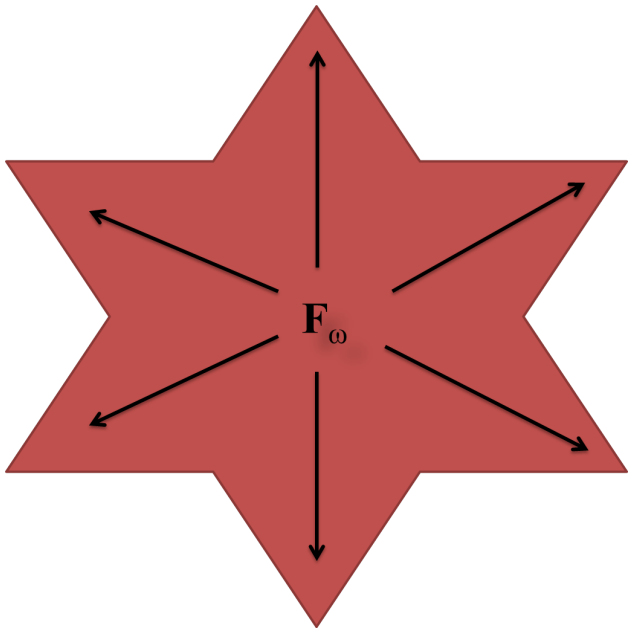

Figure 6.2: Due to the fact that the centrifugal force acts evenly in all directions from the centre it is possible to deliver the sample simultaneously down each of the 6 chambers located at each point of the star with great accuracy and without any flow-rate variation that might occur in a pumped or flow-based system .

The first step was to design a central reservoir that would enable the unhindered passage of cells and beads from the macro-sized central unit down to the microchannels which constituted the magnetophoretic section of the disc. After several iterations of designs (Solidworks, USA) of varying shapes and sizes a 6 pronged "starfish" inspired design was chosen (Figs. 6.1 and 6.2) . The gently sloping edges and sharp corners ensured that clogging or trapping of cells and beads was kept to an absolute minimum while they were moved from centre to edge. The method of manufacture of this disc was to once again be in PDMS which was necessary to form the small channels needed as well as to enable the degas driven flow that is necessary to fill the chambers for the stopped-flow system. However, purely photolithographically manufactured channels would not be possible as the height dimensions of the central reservoir were orders of magnitude too large. The chosen manufacturing technique for this part was 3-D printing (Uprint, USA). 3D printing

enabled the rapid prototyping of several different designs and enabled creation of structures of sufficient size and resolution for our purpose. A method of integrating the 3D printed part with the photolighograpically constructed section was then developed and can be seen in figure 6.3.

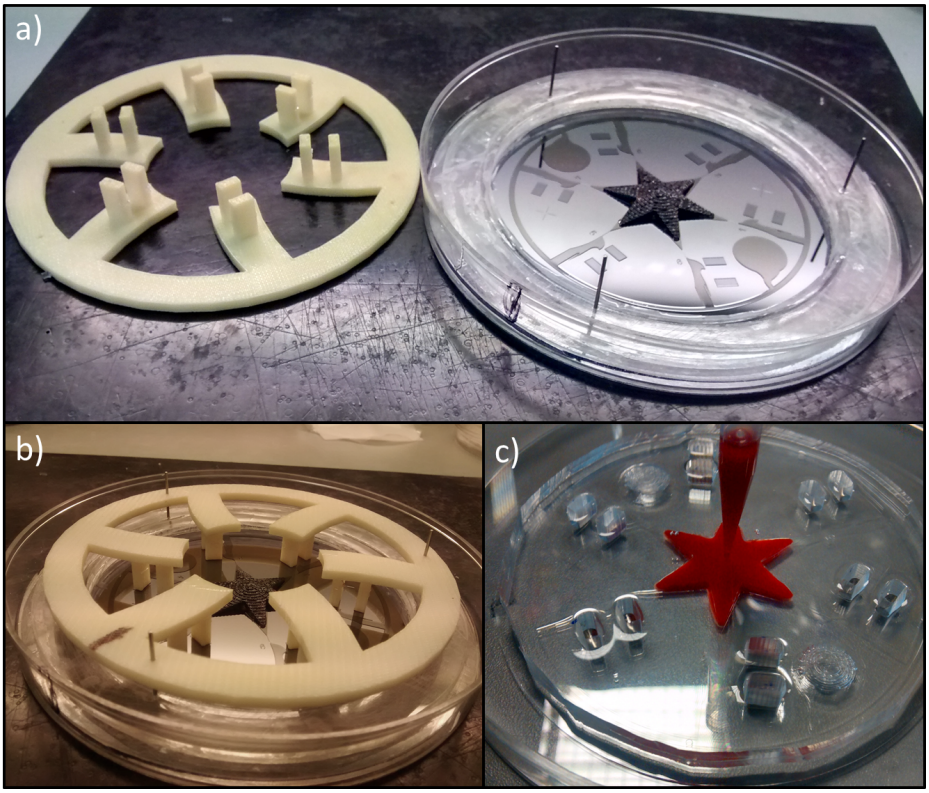

Figure 6.3: a) The 3D printed magnet positioning mould is seen on the left (white), while the photolithographically manufactured master with the adhered 3D printed central structure (black) is on the right. b) After being mounted on top of the master *via* the alignment pins, the PDMS can now be poured to form the negative of both 3D printed moulds and the pholitithographically formed microchannels. c) The completed PDMS disc, being loaded with a blood sample. Visualisation of chambers is clearer in fig 6.1.

6.2.2 Integration of 3D and photolithography for PDMS casting

Simple adhesion of the 3D printed part to the photolithographically constructed master was not favourable due to the irreversible nature of the bond and the propensity for damaging or at least contaminating the master with overspill necessary to ensure the whole bottom surface formed a tight seal with the master below.

Instead, a method of bonding with red PDMS was developed. This turned out to be ideal as red PDMS could also be used to coat the part to give a smoother finish and to reduce any adhesion of the clear PDMS to the 3D printed part during the curing process as red and clear PDMS do not bond to each other once one is cured. Red PDMS was mixed with curing agent at a ratio of 10:1. A small amount of red PDMS was applied to the bottom surface of the 3D printed part. The part was then placed onto the centre of the master and adjusted until it lined up perfectly with the SU-8 structure below it. The whole structure was then put in an oven at 70°C for 15 minutes to allow the red PDMS to fully cure. A reversible bond was now formed between the master and the 3D printed part. Any excess red PDMS could also be easily trimmed away with a scalpel blade and would easily peel away from the surface. The bond between the 3D-printed part and the master was robust enough to last for over 100 casts but could easily be broken by simply twisting the part. This enabled new 3-D printed designs to be tested without having to construct a new master, which would have been significantly more time consuming.

A 3D printed jig was also fabricated to allow the disc to be loaded on the motor as it could not have a centre hole, like the previous designs. This jig enabled the disc to be held from the outside of the disc and then centrifugally spun.

6.2.3 Binding of beads and cells

The same principle of binding of anti-EpCAM functionalised magnetic beads to MCF7 cells spiked into blood described in chapter 3.2.3 was used to prove

the functionality and determine the efficiency of the device before any patient sample could be tested. However due to the increased sample volume there were some slight differences. Blood was extracted from the arm of a healthy donor into a 3ml BD EDTA vacutainer (Becton, Dickinson and Company, USA). 200μl of the blood was placed into an eppendorf tube. 5μl of anti-EpCAM functionalised magnetic dynabeads (CELLection, Epthelial enrich, Dynabead) and the required concentration of MCF7 cells were added to the blood sample. The sample was then incubated for 20 minutes on a rotator at room temperature. The sample was now then ready to be loaded onto the disc for centrifugation.

6.2.4 Loading procedure for "starfish design"

In order to facilitate an efficient and effective loading of sample into the central loading chamber it was necessary to devise a new method of introducing sample into the system. In chapters 2 and 3, loading was done in a loading chamber that had a vent and an inlet. The vent could not be upstream of the inlet or flow could be induced during rotation. To that end, the vent was located at the same radial position a few milimetres away from the inlet. This led to a not insignificant amount of sample being lost by travelling back up the vent during loading. This was accepted as systematic loss. However, this problem was rectified in this design. The idea was to have no vent, only one loading hole (Fig 6.3 c). Once the disc had been filled with buffer by degas flow it was necessary to load the 200μl blood sample. In order for this to happen, 200μl l of buffer would have to be removed.

To facilitate a sample loading procedure that minimised loss and introduction of bubbles, the loading procedure outlined in Fig 6.4 and visible in Fig. 6.3 c) was carried out.

6.3 Experimental procedure

Once the central loading chamber was filled with the blood/bead/cell mixture it could be placed on the motor and spun at the required spin frequency.

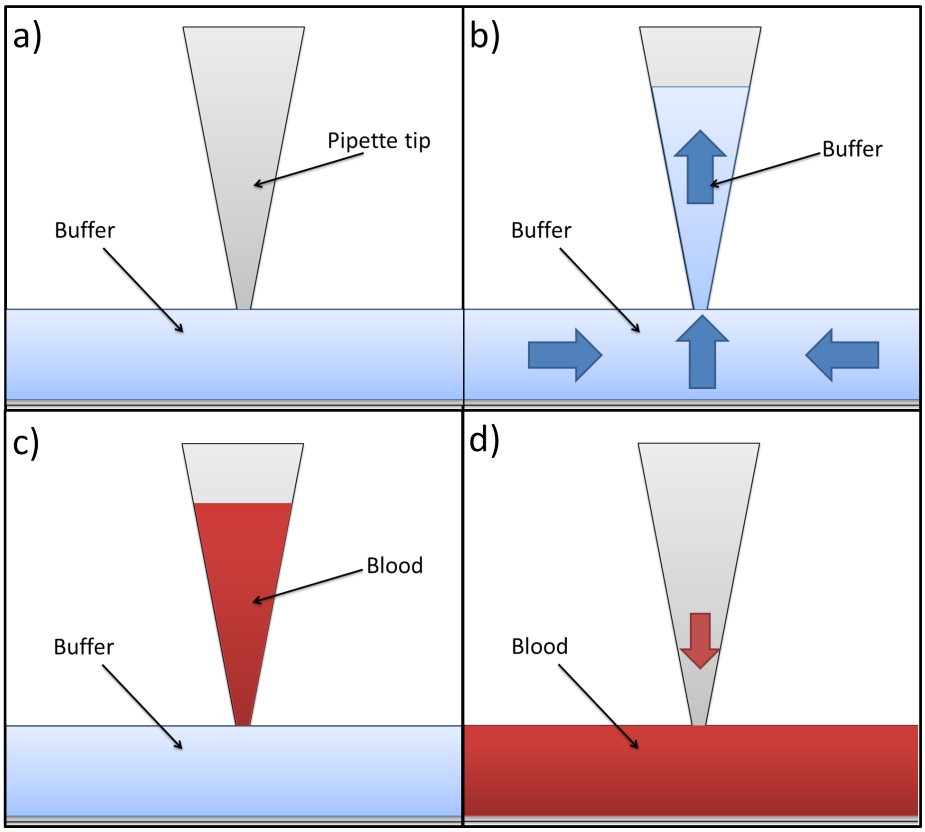

Figure 6.4: The loading procedure which can be seen in figure 6.3 c) is outlined here. a) A P1000 pipette tip was wedged into the 1mm diameter inlet in the central reservoir. b) A positive pressure is applied by depressing the "bladder" type structures near the edge of the disc, causing buffer to flow up the pipette tip. c) The buffer the tip is replaced with the blood sample. d) The "bladder" structures are released and a negative pressure draws the blood sample back into the loading structure, refilling it for stopped flow sedimentation.

After several iterations of different spin frequencies which resulted in large losses of target cells, or contamination of the capture chamber with blood cells due to turbulent effects caused by the increased rate of mass transfer into the chamber (Discussed in more detail in "turbulence problems" section) the optimum frequency was found to be 17.5hz.

6.3.1 Issues with turbulence

One problem that immediately became apparent with the almost 2 orders of magnitude increase in volume was the fact that millions more cells and beads were having to travel down the focusing channel and into the separation chamber than during the experiments in chapter 3. This was detrimental to the stopped flow nature of the device as it caused a turbulent flow to be initiated in the channel. Briefly, whenever a particle passes from the centre towards the edge of the disc through the stationary liquid, it must displace a certain volume of that liquid, dependent on its own volume. This effect is negligible in the lower volume systems discussed in chapters 2 and 3. It even slightly helps to enhance the system by offering some slight particle focusing effects on the blood entering the channel (See Fig. 3.2) due to a very slight backflow of the displaced liquid. However, when the amount of mass (cells and beads) entering the separating chamber becomes too high the amount of "backflow" becomes distruptive to the sedimentation of the particles and can cause turbulence and dispersion. This led to the defined limit of 200μl of blood being loaded in the central chamber and the optimal spin speed of 17.5 Hz being determined so as to minimise the turbulent effects caused by the large amount of cells sedimenting through the system at high speed.

6.3.2 Centrifugation

As already highlighted in the introduction, this design was chosen to utilise the fact that the centrifugal force acts equally in all radial directions from the centre of the disc. This allowed the sample (in this case blood, beads and cells) to be sedimented uniformly through all chambers on the disc simultaneously. This method of moving the sample from centre to edge while passing all six magnetophoretic chambers can be clearly be seen in Fig 6.5.

This was a 200μl blood sample containing MCF7 cells and magnetic tagging particles that was loaded into the centre of the disc by the method outlined in experimental procedures section below. It was then spun at 17.5hz for one hour to allow the full sample to sediment through (However, the magnetic particles are captured in a matter of minutes).

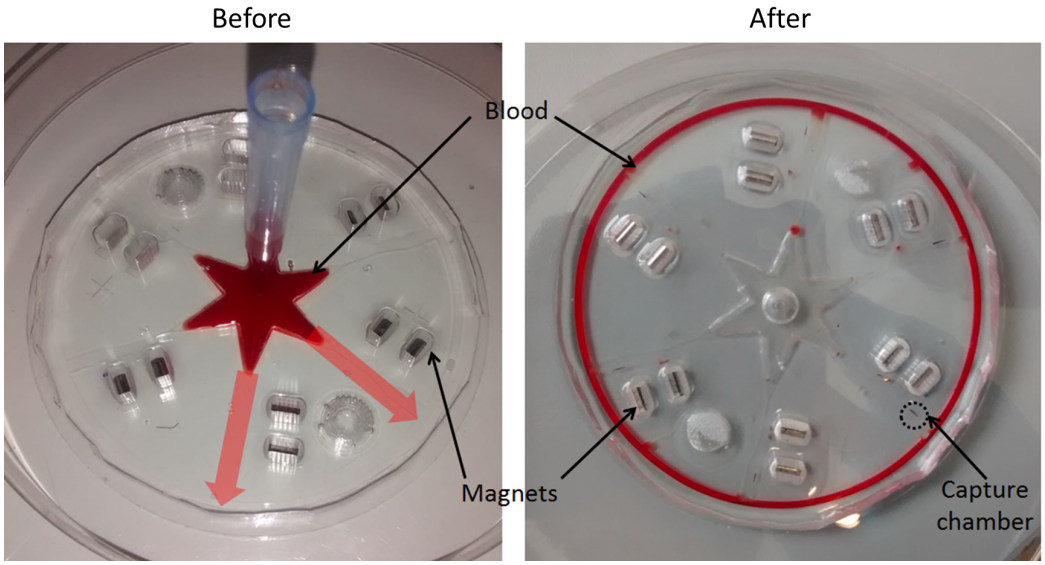

Figure 6.5: Photo of the high volume "starfish" design before and after rotation at 17.5hz. The blood sample has travelled from the centre, right to the edge, undergoing stopped-flow magnetophoresis in each chamber simultaneously.

6.4 Results

Since this system was able to process 200μl of blood, it was possible to decrease the concentration of spiked MCF7 cells significantly to significantly more realistic patient volumes [7] now that the disc was able to handle 200μl of blood. The system was found to reliably detect MCF7 cells spiked into blood at concentrations from 100 cells/μl right down to 0.1 cells/μl. A visualisation of this in one of the capture areas with fluorescently tagged MCF7 cells that were spiked into a 200μl blood sample at a concentration of 1 cell/μl is seen in Fig. 6.6 which outlines the proof of principle of the successful capture of these spiked cells while the more detailed data is presented in Fig 6.7 and 6.8.

The graphs in Figs 6.7 and 6.8 display the number of MCF7 cells detected on discs against the original spiked concentrations.

Fig. 6.7 shows the cells captured at the lower concentrations, while Fig. 6.8 includes a sample with a much higher concentration, to see if the linear

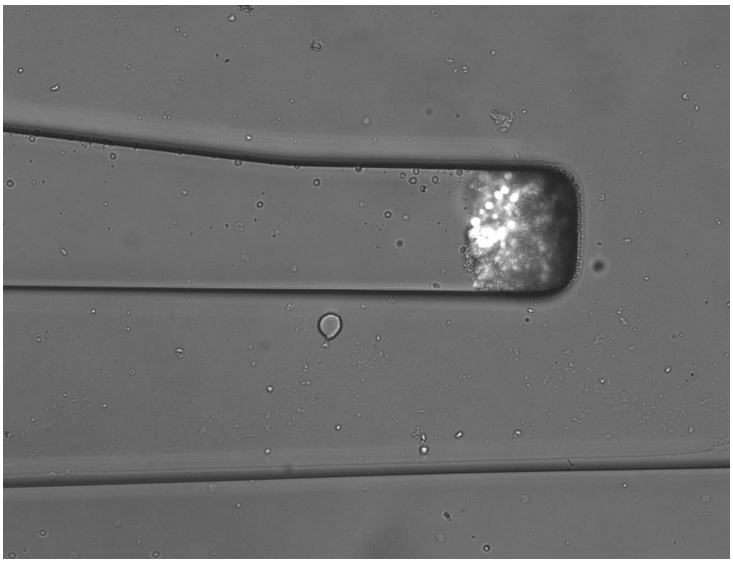

Figure 6.6: Microscope image of captured MCF7 cells in one chamber of the "starfish" disc. This demonstrated that the system was able to be loaded with 200μl of blood that had been spiked with MCF7 cells at a concentration of 1 cell/μl and successfully detect the spiked cells.

relationship was maintained. An excellent linear relationship was shown in both cases.

6.5 Conclusions and outlook

An increase of sample volume of almost 2 orders of magnitude to 0.2ml by integrating several manufacturing techniques and a limit of detection improvement of one order of magnitude over the initial work in this thesis was shown for a centrifugal magnetophoretic stopped-flow lab-on-a-disc platfrom. Detection of spiked cancer cells from blood was now being done at the high end of the clinically relevant spectrum, and on a novel and simplistic microfluidic device.

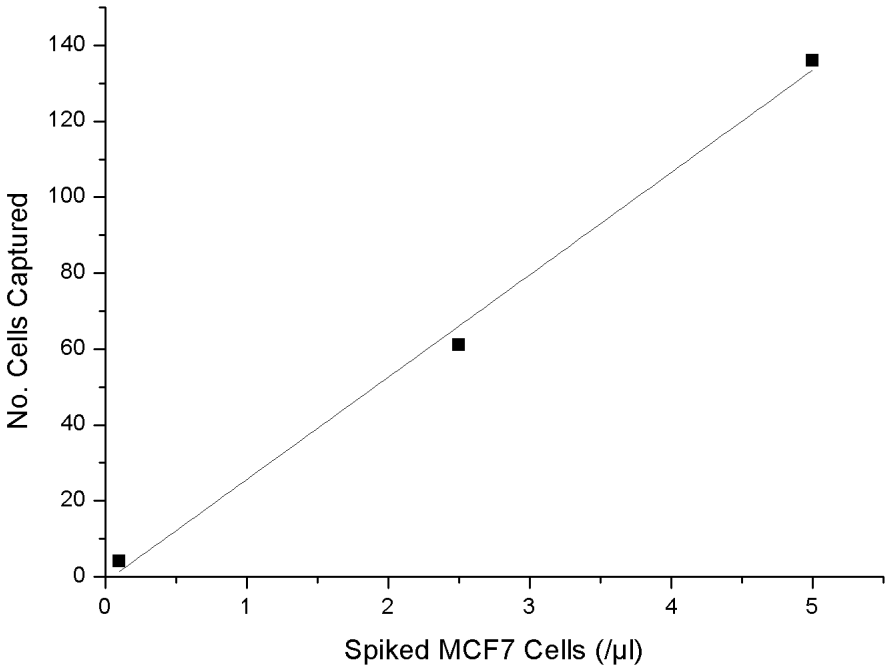

Figure 6.7: Graph showing the capture of MCF7 cells at three different concentrations in 200μl of blood. A clear linear relationship can be seen with an R^2 value of 0.995. The limit of detection in this case is an order of magnitude lower than the system in chapter three.

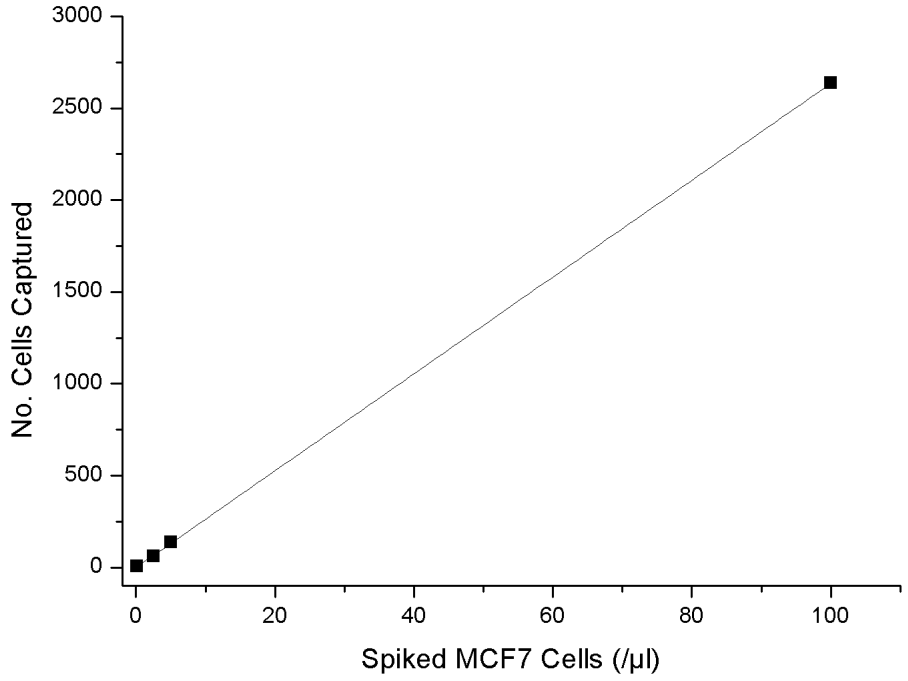

Figure 6.8: A higher concentration of 100 MCF7 cells/μl was also included to see if the linear correlation continued. A clear linear relationship can be seen with an R^2 value of 0.99. This shows a highly reliable system for a whole range of cell concentrations in a 200μl blood sample.

Chapter 7

Density Based Blood Cell Enrichment in a Stopped-Flow System

This chapter is based on the following publication:
Continuous, stopped-flow separation for integrated blood cell enrichment and analysis on centrifugal microfluidic platforms
Daniel Kirby, Claire O'Connell and Jens Ducrée,
Proceedings of the 4th European Conference on Microfluidics - Microfluidics 2014 - Limerick, Ireland. December 10-12, 2014.

As a solution for solving the volume problem for CTC detection, it was envisaged to develop a method of isolating mononuclear cells (white blood cells, CTC's or spiked cancer cells) from red blood cells as a form of on-disk sample enrichment on a stopped-flow platform. The proof of principle was proven with polystyrene beads as with the previous chapters.

Separation of microliter volumes of blood into its constitute parts is widely needed for many biological assays. This work focuses on a simple method of separating pseudo-white blood cells (PWBC's) from pseudo-red blood cells (PWBC's) based on density in a stopped-flow centrifugal platform and routing the separated PWBCs to a dedicated capture chamber. The initial inspiration for this idea came from a publication by Haeberle *et al.* where plasma was extracted from blood in a flow-based centrifugal platform [34]. However, in keeping with the stopped-flow theme of this thesis, the work described in this chapter is carried out without any fluid flow in the system, and is designed to allow for isolation of WBC's, not plasma. Polystyrene microbeads of different densities are used as biomimetic WBCs and RBCs. A separation of these pseudo cells was then performed in a stopped-flow centrifugal microfluidic disc (Fig. 7.1). After several iterations of chamber geometry, the separation was achieved by using a rounded separation unit that allowed the less dense polystyrene beads to be pushed radially inwards, layer by layer on top of the more dense red beads until they overflowed into a PWBC capture chamber. The purity of WBC-mimicking beads in the capture chamber was 97-99%. However with further testing and optimisation of the separation unit design this could be improved. If this disc design was tested with real blood samples and proved successful in separating RBCs from WBCs, then this simplistic separation unit could be a useful tool when WBC counting and analysis is desired on a stopped flow system. It could easily be incorporated into many other existing blood handling microfluidic centrifugal discs, removing the need for complicated off-disc blood handling processes and cutting the time it takes for blood analysis and blood based assays.

7.1 Introduction

Centrifugal Lab-on-a-Disc (LoaD) platforms have the innate capability of rotationally induced sedimentation of particles and other particle handling and analysis techniques [18]. However, once sedimented into a compacted volume resting on the disc, these cells are hard to retrieve for subsequent steps in an automated, multi-stage sample-to-answer cell analysis system. To this end, a continuous particle transport strategy where the cells of interest are permanently moving under the impact of a centrifugal field was envisaged.

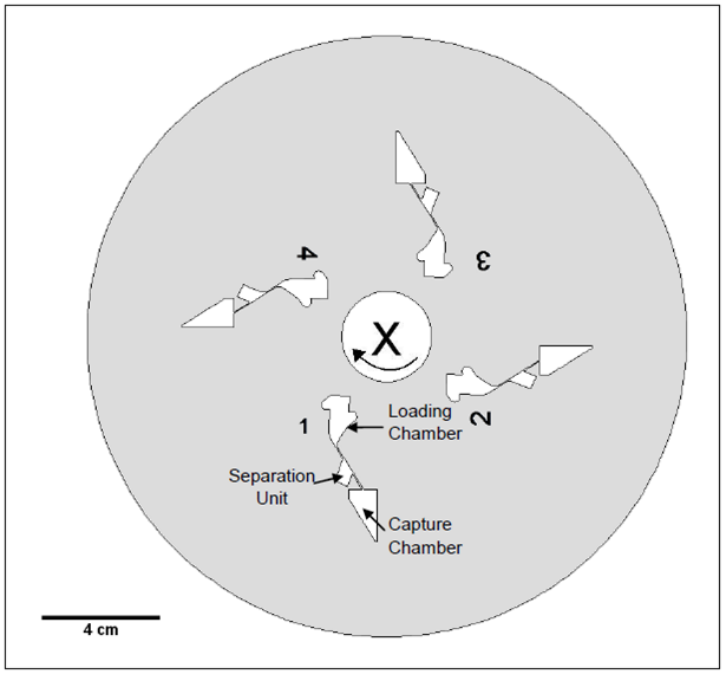

Figure 7.1: Schematic of the centrifugal microfluidic platform with the X showing the centre of rotation while the three main features of the separation structure are indicated. Four identical chambers are present on the disk for multiplexing.

This work outlines a new method for continuous particle separation under stagnant liquid conditions through rotationally induced sedimentation. A mixture of polystyrene microbeads (Microparticles GmbH) of two different densities, simulating the density difference between red and white blood cells, are driven through a stationary carrier fluid by a centrifugal field into

a separation chamber (Fig. 7.2). This chamber exhibits a volume and geometry which is designed to retain the denser red beads while passing on a high-purity (99%) sub-population of less-dense yellow beads to a downstream collection chamber where they are amenable to integrated downstream analysis and/or enumeration.

Whereas WBC isolation has been shown before in flow based microfluidic systems [87, 88], the work presented in this chapter is of paramount importance for developing methods of purifying blood samples in stopped-flow centrifugal microfluidic systems such as those discussed in the previous chapters and potential devices in the future of this under-explored field. The stopped-flow centrifugal platform lends its self well to a density based separation technique due to the fact that cells and particles can be controlled solely by the centrifugal field and independent of flow, unlike the vast majority of microfluidic devices.

7.2 Theory

It is a well-established fact that when blood is placed in a centrifuge it can be fractioned into its component parts in order of density. Our work used this principle to develop a method of spatially separating particles of different densities to individual chambers on a stopped flow centrifugal microfluidic platform. The accepted values for the density of red blood cells are $1139 \pm 3kg/m^3$, white blood cells are $1080 \pm 5Kg/m^3$ [31, 89]

As can be seen in figure 7.3, the mixture of particles will enter the separation unit from the left and more dense particles will sediment to the bottom, while pushing the less dense particles to the top where they can over flow to the capture chamber at a different radial position on the disk. The key parameters which govern the efficiency of the system are the angle of the inlet channel, the size and geometry of the separation unit and the angle at which that structure is placed. After initial work with the basic geometry seen in figure 6.3, the optimal geometry visible in figure 7.4 was discovered.

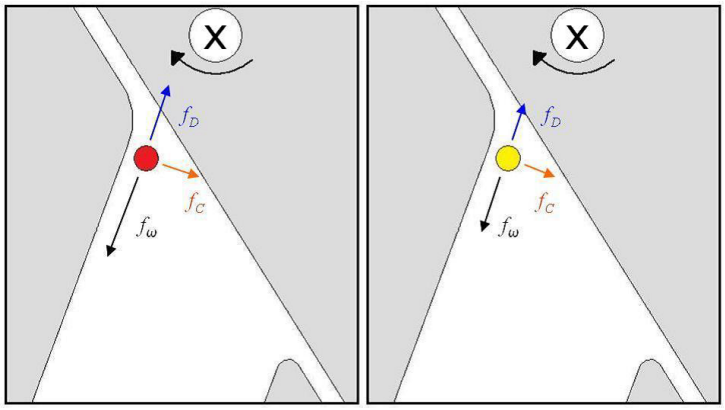

Figure 7.2: Schematic of the entrance of the separation unit with relative forces indicated for both high density beads and lower density beads. Where (f_ω) is the centrifugal force, (f_c) is the corialis force and (f_d) is the stokes drag. Direction towards centre of rotation is indicated by "X".

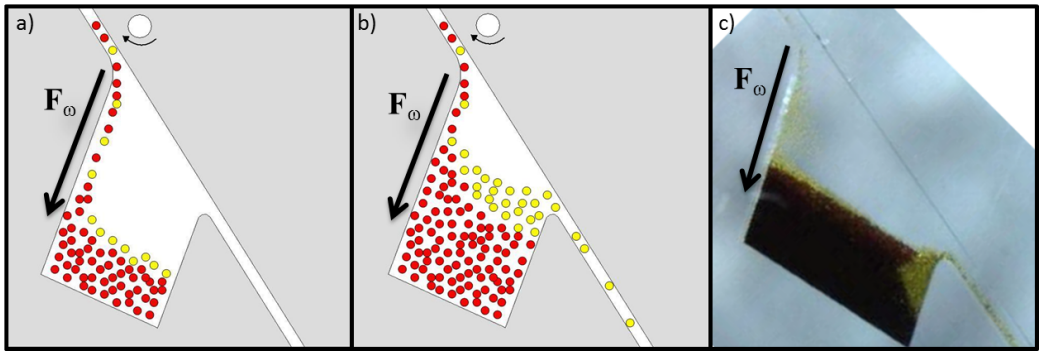

Figure 7.3: a) Schematic of high density (red) and less dense (yellow) microbeads entering the separation unit. b) As the chamber fills, the more dense red particles should sediment to the bottom, while the less dense yellow particles move to the top (or radially inward location) and overflow into a capture chamber. c) In practice it was found that the chamber geometry was trapping many yellow particles against the right-hand wall and leaving many more stranded near the left-hand wall. A redesign was necessary

7.2.1 Final design of separation unit

The initial designs all ran into problems with trapping the majority of the low density particles against the side walls. So, after several design iterations, a curved shape with one inner side parallel to the centrifugal force vector was found to be optimal as this allowed the denser red beads to sediment

to the bottom while the less dense yellow beads were carried along by the centrifugal force to a separate chamber (Fig 7.4).

Figure 7.4: Schematic of the optimal design of the separation unit which allowed the less dense beads to freely move to the top of the more dense red beads and escape towards the capture chamber.

7.3 Materials and methods

The discs were manufactured in PDMS, by soft lithography in an almost identical fashion to the platforms already discussed in earlier chapters. However, in brief, the disks designs were drawn on AutoCAD (Autodesk Inc.) and were manufactured using standard UV lithography and cast in polydimethylsiloxane (PDMS). The 100mm diameter base of the disks were cut from PMMA using a C02 laser and assembled by spin-coating the PMMA with a thin layer of PDMS to allow for thermal bonding between the top and bottom layers of PDMS. The two types of polystyrene particles used were yellow 20m polystyrene particles with a density of 1.05 g/cm3 (used to simulate WBCs) and red 20m polystyrene particles with a 20% iron core and density of 1.88g/cm3 (used to simulate RBCs).

7.4 Results

During centrifugation, a continuous stream of particles enters the separation chamber (Fig. 7.5). Due to their higher density, the red beads seek to fill the separation chamber along its radially outer wall, while the less dense

yellow beads remain on top. The continuous nature of this particle separation (i.e. cells entering in a straight line, not a bulk migration as in a standard centrifuge tube) prevents entrapment of the yellow beads in the stream of abundant red beads. Due to the above mentioned factors the device gives an extremely high purity (99%) of the yellow population (Fig. 7.6). The percentage of yellow beads left behind in the separation unit was found to be less than 10%. However, the design of the separation unit may be specifically optimised for either a high yellow bead purity (by accepting by a small loss) or a high retrieval efficiency (by accepting a slight impurity of red beads).

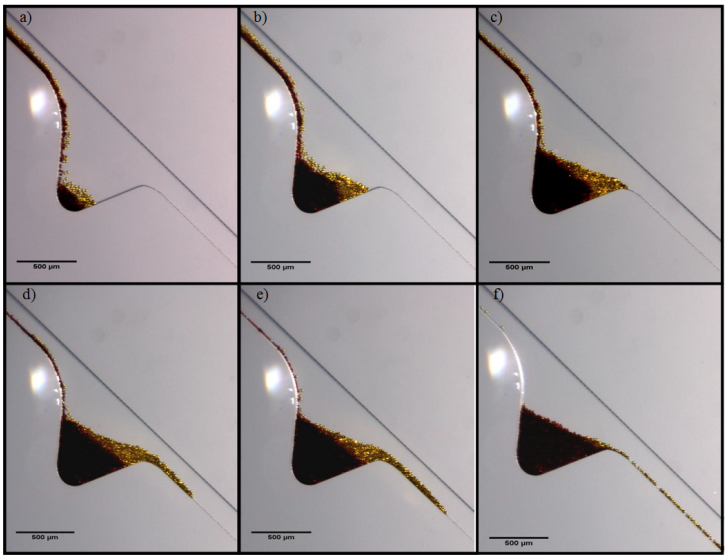

Figure 7.5: a) Image of mixed red and yellow beads entering the separation unit with a lateral density gradient already visible. b e) As the chamber fills up the less dense yellow beads are continuously pushed along the curved edge of the separation unit towards the overflow channel, where they continue towards a separate retention chamber. f) The input sample has been metered to ensure that only the yellow beads will reach the overflow channel. Incorrect metering would lead to a red bead contamination in the capture chamber.

7.5 Conclusion

Pseudo blood cells were simulated using 20m yellow polystyrene beads to represent white blood cells and 20m red iron core polystyrene beads to rep-

Figure 7.6: Routing of isolated yellow beads to the capture chamber with a purity of 99%.

resent the more dense red blood cells. A separation of these pseudo cells was then performed in a stopped-flow centrifugal microfluidic disc. The separation was achieved by using a rounded separation unit that allowed the less dense polystyrene beads to be pushed radially inwards, layer by layer on top of the more dense red beads until they overflowed into a capture chamber. The purity of yellow beads in the capture chamber was 99% at a 1:1 ratio of red and yellow beads and for the 4:1 mixture it was 97%. However with

further testing and optimisation of the separation unit design this could be improved. While it must be admitted that the density difference between the red and yellow beads is significantly greater than that between red blood cells and mononuclear cells and that the concentrations of these beads are a long way from a real blood sample, the principle of density based separation of microparticles on a stopped-flow system was successfully shown. If an advanced version of this disc design was tested with real blood samples and proved successful in separating RBCs from WBCs, then this simplistic separation unit could be a useful tool when only WBC (or CTC) counting and analysis is desired on a stopped flow system. It could easily be incorporated into many other existing blood handling microfluidic centrifugal discs, removing the need for complicated off-disc processes and cutting the time it takes for blood analysis and blood based assays.

Chapter 8

Magnetic teardrops

This chapter is based on the following publication:
Reversible imunomagnetic cell trapping and analysis on an array of thin-film permalloy microfeatures,
Daniel Kirby, Eanna Bailey, Macdara Glynn, Charles Nwankire and Jens Ducrée,
Proceedings of 18th International Conference on Miniaturized Systems for Chemistry and Life Sciences (μTAS) October 26-30, 2014, San Antonio, Texas, USA.

It is important to note that the work in the following chapter was carried out "on-chip" as a proof of principle and was in fact the only work not undertaken on a centrifugal platform.

Isolation and individual analysis of target cells from a bulk sample is vital in cell-based diagnostics. Previous work from Burger *et.al* [26] outlined a method of trapping microparticles in a highly ordered array of geometrical barriers, termed "v-cups". However, any geometrical barriers, especially ones that are highly ordered and close together are highly susceptible to clogging, especially if there are no divergent flow lines around the barriers, as in a stopped-flow system. The concept for the work in this chapter was to create an array of "virtual v-cups" by patterning dots of ferrous material on the floor of a microchannel. Upon exposure of the microchannel to an external magnetic field, the field intensity would be increased in the areas patterned with the ferrous material. This would create a pattern of magnetic "potential wells" where a magnetic particle or magnetically tagged cell at a close enough vicinity would migrate to. By patterning an array of these "magnetic dots" on the floor of a channel a barrier-free completely open channel would be able to retain cells or particles in much the same way as the v-cups but with no clog-causing barriers and with the possibility of releasing the cells for downstream analysis by merely removing the external magnetic field. We here present the magnetically controlled separation of specific target cells by a sputter-deposited thin-film of permalloy teardrops. Apart from simplified fabrication of our essentially 2-dimensional (160nm thick), thin-film architecture, our device also features high capture efficiencies, leaves flow lines unperturbed, assures homogeneous reagent exposure and suppresses particle clogging. Furthermore, the trapped cells can readily be released for further downstream analysis by removing the external magnetic field, thus fully regenerating the device for the next experiment.

8.1 Introduction

Capture and analysis of individual cells from a mixed population is vital in cell-based diagnostics. Previous work has established the ability to array target cells using 3-dimensional geometrical obstacles such as micropillars and cups [1]. We here present a separation device that aligns magnetic beads and immuno-magnetically tagged target cells into an ordered grid generated by a micropatterned, 160-nm thick permalloy film (80% Nickel, 20% Iron) deposited on the base of the chamber (Fig. 8.1).

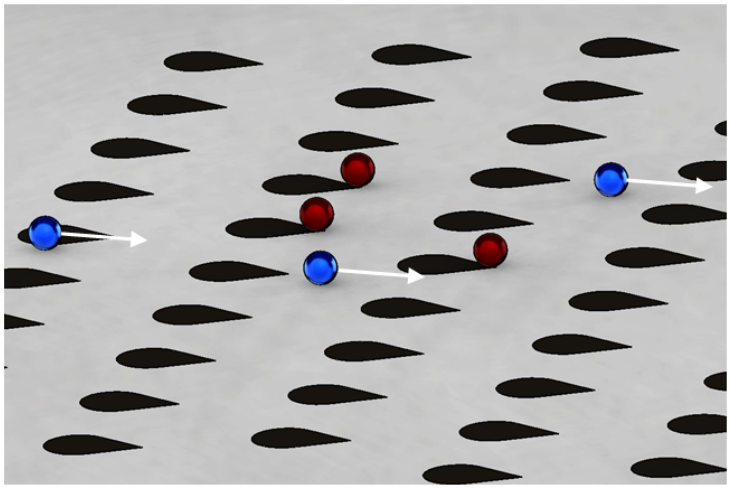

Figure 8.1: Magnetic bioparticles such as beads or tagged cells (red) are retained at the tip of the teardrop-shaped magnetic dots (black) where the local field is strongest while the unperturbed, non-magnetic particles (blue) continue in the downstream direction.

Maxima of the magnetic field arise in the vicinity of the sharp edges of these microfeatures, as outlined in the magnetic field simulations (Fig. 8.2). These potential wells serve to localize paramagnetic bioparticles (within a certain size range) such as tagged cells or beads during analysis or successive steps of washing and reagent exposure. Going beyond the capabilities of geometrical barriers, our trapping mechanism is inherently reversible and can be easily adapted to suit specific particle sizes or flow conditions.

Magnetic cell isolation has become widespread, with the majority of systems using bulk magnetic forces [90]. The novelty in our system is the arrayed

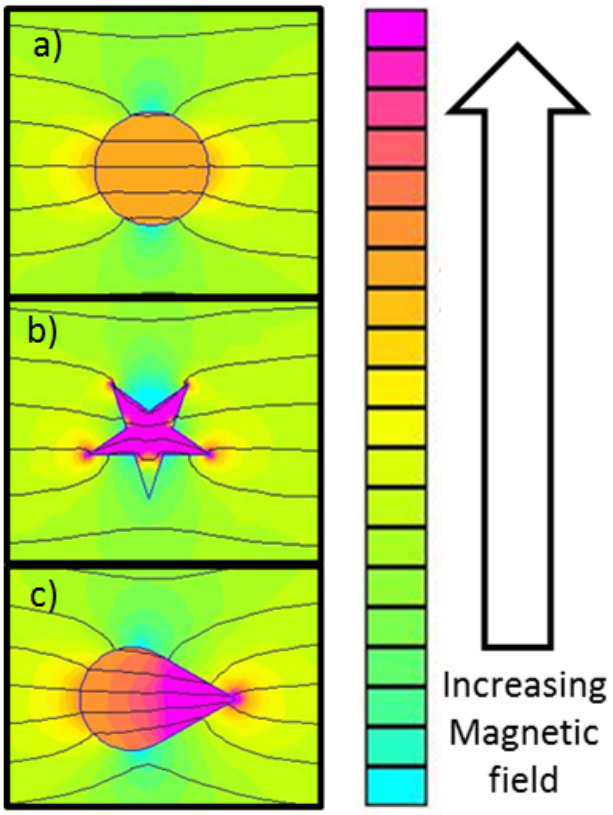

Figure 8.2: Simulation of local magnetic field for different shapes of a micropatterned permalloy film in a uniform external magnetic field. a) The round dot delivers a rather even distribution of the magnetic field. b) The star-shaped structure provides a larger field amplitude but it features several maxima. c) The teardrop shape focusses the magnetic field in into a single maximum which turned out to be optimal for capture of individual bioparticles at high spatial definition.

trapping of the magnetically tagged cells (Fig. 8.3) where they can be studied individually and undergo media change, e.g. for fluorescent staining [26]. The thin-film nature of these traps suppresses clogging and inevitable divergence of flow lines around 3D-obstacles, thus enhancing capture efficiency and assuring uniform exposure to reagents. Following on-array retention, the cells can be efficiently released into a downstream capture chamber by simply removing the magnetic field.

8.2 Materials and Methods

The permalloy features are deposited on the floor of the chip by sputter-coating a UV-lithographically patterned (OAI, model 200) AZ-photoresist which was spin-coated on glass slides. A PMMA lid was cut by a CO2 laser and bonded to the glass via a pressure-sensitive adhesive featuring an 86μm high microchannel for the passage of the cells. The MCF7 cancer cells were incubated with 4.5μm magnetic anti-EpCAM beads before being introduced to the system.

8.3 Results

This chip enables the separation of target bioparticles from an abundant background into an array of magnetic traps with single-occupancy distribution (Fig. 8.3a & b). We have measured a capture efficiency of over 99% for magnetic beads and a purity of 98.5%, with a non-magnetic particle purity of over 99.9% in the waste chamber.

With a biomimetic sample of magnetically tagged MCF7 cells spiked into whole blood, we have furthermore shown a capture efficiency of 100% (Fig. 8.3c) while over 99% of the background blood cells advance to the waste chamber. We have also demonstrated media exchange without disturbing the retention of the cells and successfully released them for downstream analysis. We have also performed size separation by the variation of micro-dot geometry. Overall, this new and reversible magnetic alignment method of individual cells could easily be adapted to various formats of particle-based bioassays.

8.4 Conclusion

We have shown an immuno-magnetic method for high-efficiency, reversible trapping of magnetically tagged target cells suspended in a biological background into an array where they can be analysed by common bioanalytical protocols. The 2-dimensional nature of the system facilitates microfabrica-

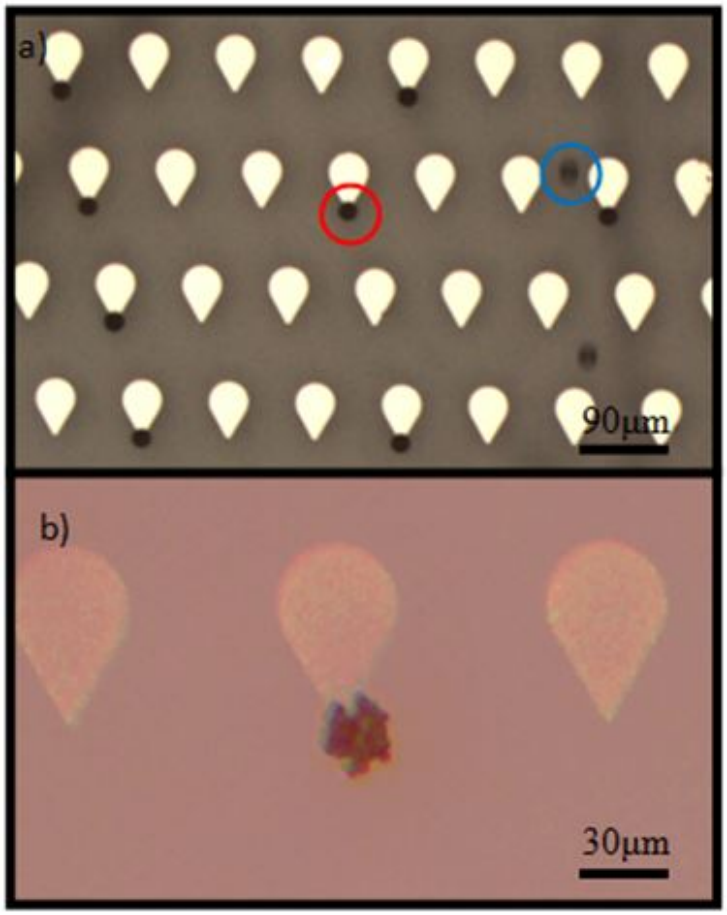

Figure 8.3: a) Microscope image of 20μm magnetic beads (red circle) trapped by the local magnetic field maxima at the tips of the magnetic permalloy teardrops while the trajectory of non-magnetic beads (blue circle) remains unperturbed. The magnetic beads were captured with a sensitivity of 99.6% and a purity of 98.5%. Also, 99.95% of the non-magnetic beads were routed to the waste chamber. b) Magnetically tagged MCF7 cells were trapped on the magnetic permalloy teardrops, formed using an OAI 200 mask aligner.

tion, suppresses issues such as particle clogging and diverging flow fields that occur with common, 3D-geometrical obstacles and thus enhances capture efficiency. It is in the very early stages, but if integrated into a stopped-flow microfluidic device it could offer an attractive method of arraying and analysing magnetically tagged cells.

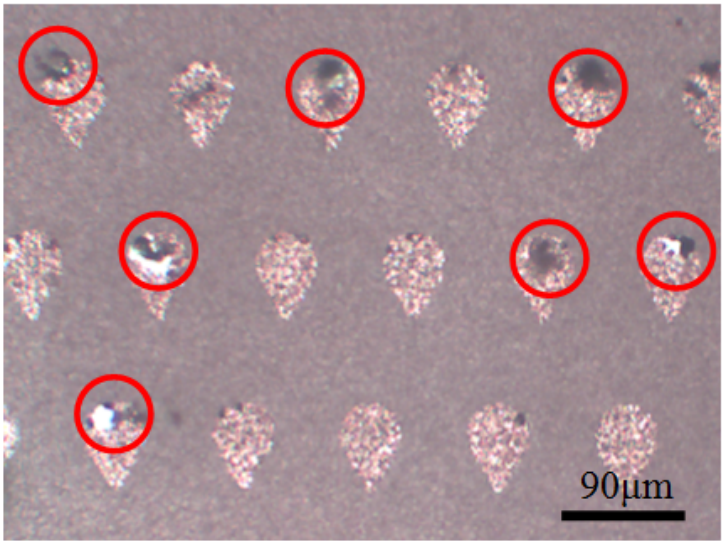

Figure 8.4: Capture of tagged MCF7 cells (circled in red) in a background of whole blood, which is flowing past. The MCF7 cells were captured with a sensitivity of 100%, while over 99% of the blood cells were routed to the waste chamber.

Chapter 9

Conclusions and future work

This thesis outlines the work undertaken towards completion of a PhD on the topic of magnetophoretic cell handling on a centrifugal microfluidic platform for rare cancer cell detection in blood. Circulating tumour cells are currently not detectable in any standard clinical or hospital setting. Developing a system that would enable this would be a serious game-changer in cancer diagnosis and prognosis. This work focuses on outlining from a physical, biological, clinical and engineering perspective, the development of a microfluidic device for circulating tumour cell (CTC) detection. At first the physical principle was shown by using bio-mimetic polystyrene microbeads to simulate cancer cells in blood. This process began by developing a system that could separate and detect a rare concentration of magnetic microbeads in an abundant background of non-magnetic microbeads with an sensitivity of over 96%. It is important to note that this was the first published case of lateral magnetophoretic separation of particles on a centrifugal platform. One of the key factors in the accuracy and simplicity of this technique was the stopped-flow system which was used. Stopped-flow enables far higher levels of control over particles' trajectories than in a standard flow-based microfluidic platform which contains divergent flow lines and varying flow profiles. Once the bio-mimetic section of the work was completed, an investigation into using a real biological sample was undertaken. This resulted in using magnetically tagged MCF7 breast cancer cells spiked into a blood sample

with the understanding that they should behave in a very similar fashion to the biomimetic microbeads. After various iterations of optimisations and adjustments this indeed proved to be the case, and as well as successfully capturing magnetically tagged cancer cells in a blood background at a concentration of as low as 1 cell/μl and with a sensitivity of over 80%, a method of brightfield enumeration of the captured cells was also developed which enabled the author to easily differentiate between a healthy blood sample and blood containing 5 different concentrations of MCF7 cancer cells.

Once this stage in the research was completed, the work could advance towards being more clinically relevant. The first step was to redesign the system to handle volumes on the millilitre scale, as opposed to the microlitre scale. This required integration of various manufacturing techniques and led to new problems in maintaining a stable stopped-flow magnetophoretic system due to the massive increase in material being passed through the channels. However once these new hurdles were crossed the author was able to successfully analyse 0.2ml of blood and detect cancer cells at a concentration of as low as 0.1 cell/μl as opposed to 1 cell/μl in a 3μl sample, which was the maximum sample volume at the initial stage of the work. This almost 2 orders of magnitude shift in the volume capabilities along with an order of magnitude improvement in the limit of detection of the device moved it into the region where true analysis of clinical samples could be possible.

If this work was pushed to the next level by investigating further the complex properties of circulating tumour cells and tailoring the capture parameters of this our system to same, then a truly bedside CTC detection lab-on-a-disc device could become a clinical reality. This would ignite a whole new method of dealing with cancer, moving away from costly, time consuming and overburdened MRI and CT machines and making room for CTC detection from blood, right at the patient's bedside.

As well as focusing on the main topic, the author has also investigated various other methods of magnetic and stopped flow particle control for other purposes. This can be seen in the chapters on density based separation of particles for blood processing in a stopped-flow environment, virtual magnetic traps for barrier free filtration of particles or cells based on their size

and surface markers, and on the HIV-AIDS diagnostic that was developed based on the original work presented here.

It is hoped that by presenting this work on the hugely under-explored area of stopped-flow centrifugal magnetophoresis and by elucidating the many unique benefits it has, that the field will continue to grow and build on what has been shown in order to make great strides in the field of cell analysis on lab-on-disc platforms for biomedical applications.

References

[1] Cancer Factsheet - national cancer registry of ireland `http://www.ncri.ie/sites/ncri/files/factsheets/FACTSHEET_all%20cancers.pdf`.

[2] M. A. M. Gijs. Magnetic bead handling on-chip: new opportunities for analytical applications. *Microfluidics and Nanofluidics*, 1(1):22–40, October 2004.

[3] N. Pamme and A. Manz. On-chip free-flow magnetophoresis: continuous flow separation of magnetic particles and agglomerates. *Analytical chemistry*, 76(24):7250–6, December 2004.

[4] N. Pamme. Continuous flow separations in microfluidic devices. *Lab on a chip*, 7(12):1644–59, December 2007.

[5] D. Pappas and K. Wang. Cellular separations: a review of new challenges in analytical chemistry. *Analytica chimica acta*, 601(1):26–35, October 2007.

[6] E. H. Cho, M. Wendel, M. Luttgen, C. Yoshioka, D. Marrinucci, D. Lazar, E. Schram, J. Nieva, L. Bazhenova, A. Morgan, A. H. Ko, W. M. Korn, A. Kolatkar, K. Bethel, and P. Kuhn. Characterization of circulating tumor cell aggregates identified in patients with epithelial tumors. *Physical biology*, 9(1):016001, February 2012.

[7] D. Marrinucci, K. Bethel, A. Kolatkar, M. S. Luttgen, M. Malchiodi, F. Baehring, K. Voigt, D. Lazar, J. Nieva, L. Bazhenova, et al. Fluid biopsy in patients with metastatic prostate, pancreatic and breast cancers. *Physical biology*, 9(1):016003, 2012.

[8] C. Alix-Panabières and K. Pantel. Challenges in circulating tumour cell research. *Nature Reviews Cancer*, 14(9):623–631, 2014.

[9] J. Siegrist, R. Peytavi, M. Bergeron, and M. Madou. Microfluidics for ivd analysis: triumphs and hurdles of centrifugal platformspart 1: molecular fundamentals. *IVD Tech*, 15:22–26, 2009.

[10] J. Siegrist, L. Zavattoni, and J. Ducrée. Centrifugo-magnetophoretic separation and routing of particles. In *Micro Electro Mechanical Systems (MEMS), 2011 IEEE 24th International Conference on*, pages 1107–1110. IEEE, 2011.

[11] J. Siegrist, R. Burger, D. Kirby, L. Zavattoni, G. Kijanka, and J. Ducrée. Stress-free centrifugomagnetic 2d-separation of cancer cells in a stopped-flow mode. In *15th International Conference on Miniaturized Systems for Chemistry and Life Sciences (uTAS). Seattle, USA*, pages 2–6, 2011.

[12] T. Ashworth. A case of cancer in which cells similar to those in the tumours were seen in the blood after death. *Aust Med J*, 14(3):146–149, 1869.

[13] M. Cristofanilli, G. T. Budd, M. J. Ellis, A. Stopeck, J. Matera, M. C. Miller, J. M. Reuben, G. V. Doyle, W. J. Allard, L. W. Terstappen, et al. Circulating tumor cells, disease progression, and survival in metastatic breast cancer. *New England Journal of Medicine*, 351(8):781–791, 2004.

[14] J. S. de Bono, H. I. Scher, R. B. Montgomery, C. Parker, M. C. Miller, H. Tissing, G. V. Doyle, L. W. Terstappen, K. J. Pienta, and D. Raghavan. Circulating tumor cells predict survival benefit from treatment in metastatic castration-resistant prostate cancer. *Clinical Cancer Research*, 14(19):6302–6309, 2008.

[15] M. Cristofanilli, D. F. Hayes, G. T. Budd, M. J. Ellis, A. Stopeck, J. M. Reuben, G. V. Doyle, J. Matera, W. J. Allard, M. C. Miller, et al. Circulating tumor cells: a novel prognostic factor for newly diagnosed metastatic breast cancer. *Journal of Clinical Oncology*, 23(7):1420–1430, 2005.

[16] M. Wendel, L. Bazhenova, R. Boshuizen, A. Kolatkar, M. Honnatti, E. H. Cho, D. Marrinucci, A. Sandhu, A. Perricone, P. Thistlethwaite, et al. Fluid biopsy for circulating tumor cell identification in patients with early-and late-stage non-small cell lung cancer: a glimpse into lung cancer biology. *Physical biology*, 9(1):016005, 2012.

[17] F. Farace, C. Massard, N. Vimond, F. Drusch, N. Jacques, F. Billiot, A. Laplanche, A. Chauchereau, L. Lacroix, D. Planchard, et al. A di-

rect comparison of cellsearch and iset for circulating tumour-cell detection in patients with metastatic carcinomas. *British journal of cancer*, 105(6):847–853, 2011.

[18] J. Ducrée, S. Haeberle, S. Lutz, S. Pausch, F. V. Stetten, and R. Zengerle. The centrifugal microfluidic Bio-Disk platform. *Journal of Micromechanics and Microengineering*, 17(7):S103–S115, July 2007.

[19] R. Burger, D. Kirby, M. Glynn, C. Nwankire, M. O'Sullivan, J. Siegrist, D. Kinahan, G. Aguirre, G. Kijanka, R. a. Gorkin, and J. Ducrée. Centrifugal microfluidics for cell analysis. *Current opinion in chemical biology*, pages 1–6, July 2012.

[20] O. Strohmeier, M. Keller, F. Schwemmer, S. Zehnle, D. Mark, F. von Stetten, R. Zengerle, and N. Paust. Centrifugal microfluidic platforms: advanced unit operations and applications. *Chemical Society Reviews*, 44(17):6187–6229, 2015.

[21] R. Gorkin, J. Park, J. Siegrist, M. Amasia, B. S. Lee, J.-M. Park, J. Kim, H. Kim, M. Madou, and Y.-K. Cho. Centrifugal microfluidics for biomedical applications. *Lab on a chip*, 10(14):1758–73, July 2010.

[22] H.-p. Ho, P.-m. Lau, H.-c. Kwok, S.-y. Wu, M. Gao, A. K.-l. Cheung, Q. Chen, G. Wang, Y.-w. Kwan, C.-k. Wong, et al. Allergen screening bioassays: recent developments in lab-on-a-chip and lab-on-a-disc systems. *Bioanalysis*, 6(14):2005–2018, 2014.

[23] M. Grumann, T. Brenner, C. Beer, R. Zengerle, and J. Ducree. Visualization of flow patterning in high-speed centrifugal microfluidics. *Review of Scientific Instruments*, 76(2):025101, January 2005.

[24] R. Burger, I. K. Dimov, and J. Ducrée. Highly efficient single cell capturing under stagnant flow conditions on a centrifugal microfluidic platform. In *The 13th International Conference on Miniaturized Systems for Chemistry and Life Sciences (μTAS 2009)*, 2009.

[25] M. Grumann, A. Geipel, L. Riegger, R. Zengerle, and J. Ducrée. Batch-mode mixing on centrifugal microfluidic platforms. *Lab on a Chip*, 5(5):560–565, 2005.

[26] R. Burger, P. Reith, G. Kijanka, V. Akujobi, P. Abgrall, and J. Ducrée. Array-based capture, distribution, counting and multiplexed assaying of beads on a centrifugal microfluidic platform. *Lab on a Chip*, 12(7):1289–1295, 2012.

[27] R. Burger, P. Reith, V. Akujobi, and J. Ducrée. Rotationally controlled magneto-hydrodynamic particle handling for bead-based microfluidic assays. *Microfluidics and nanofluidics*, 13(4):675–681, 2012.

[28] M. A. Gijs. Magnetic bead handling on-chip: new opportunities for analytical applications. *Microfluidics and Nanofluidics*, 1(1):22–40, 2004.

[29] M. A. Gijs, F. Lacharme, and U. Lehmann. Microfluidic applications of magnetic particles for biological analysis and catalysis. *Chemical reviews*, 110(3):1518–1563, 2009.

[30] W. F. Brown Jr. Thermal fluctuations of a single-domain particle. *Journal of Applied Physics*, 34(4):1319–1320, 1963.

[31] W. H. Grover, A. K. Bryan, M. Diez-Silva, S. Suresh, J. M. Higgins, and S. R. Manalis. Measuring single-cell density. *Proceedings of the National Academy of Sciences*, 108(27):10992–10996, 2011.

[32] D. J. Beebe, G. A. Mensing, and G. M. Walker. Physics and applications of microfluidics in biology. *Annual review of biomedical engineering*, 4:261–86, January 2002.

[33] A. Manz, N. Graber, and H. Widmer. Miniaturized total chemical analysis systems: A novel concept for chemical sensing. *Sensors and Actuators B: Chemical*, 1(1-6):244–248, January 1990.

[34] S. Haeberle, T. Brenner, R. Zengerle, and J. Ducrée. Centrifugal extraction of plasma from whole blood on a rotating disk. *Lab on a chip*, 6(6):776–81, June 2006.

[35] N. Pamme and C. Wilhelm. Continuous sorting of magnetic cells via on-chip free-flow magnetophoresis. *Lab on a chip*, 6(8):974–80, August 2006.

[36] N. Pamme. Magnetism and microfluidics. *Lab on a chip*, 6(1):24–38, January 2006.

[37] X. Xuan, J. Zhu, and C. Church. Particle focusing in microfluidic devices. *Microfluidics and nanofluidics*, 9(1):1–16, 2010.

[38] M. J. Madou. *Fundamentals of Microfabrication: The Science of Miniaturization, Second Edition*. CRC Press, 2002.

[39] M. Madou, J. Zoval, G. Jia, H. Kido, J. Kim, and N. Kim. Lab on a CD. *Annual review of biomedical engineering*, 8:601–28, January 2006.

[40] R. Burger and J. Ducrée. Handling and analysis of cells and bioparticles on centrifugal microfluidic platforms. *Expert review of molecular diagnostics*, 12(4):407–21, May 2012.

[41] J. Steigert, T. Brenner, M. Grumann, L. Riegger, S. Lutz, R. Zengerle, and J. Ducrée. Integrated siphon-based metering and sedimentation of whole blood on a hydrophilic lab-on-a-disk. *Biomedical microdevices*, 9(5):675–9, October 2007.

[42] Y. Xia and G. M. Whitesides. Soft lithography. *Annual Review of Materials Science*, 28(1):153–184, August 1998.

[43] T. Thorsen, S. J. Maerkl, and S. R. Quake. Microfluidic large-scale integration. *Science (New York, N.Y.)*, 298(5593):580–4, October 2002.

[44] K. Hosokawa, K. Sato, N. Ichikawa, and M. Maeda. Power-free poly(dimethylsiloxane) microfluidic devices for gold nanoparticle-based DNA analysis. *Lab on a chip*, 4(3):181–5, June 2004.

[45] L. E. Silbert. Jamming of frictional spheres and random loose packing. *Soft Matter*, 6(13):2918, June 2010.

[46] S. Melle, M. A. Rubio, and G. G. Fuller. Time scaling regimes in aggregation of magnetic dipolar particles: scattering dichroism results. *Physical review letters*, 87(11):115501, September 2001.

[47] S. Haeberle and R. Zengerle. Microfluidic platforms for lab-on-a-chip applications. *Lab on a chip*, 7(9):1094–110, September 2007.

[48] Y.-K. Cho, J.-G. Lee, J.-M. Park, B.-S. Lee, Y. Lee, and C. Ko. One-step pathogen specific DNA extraction from whole blood on a centrifugal microfluidic device. *Lab on a chip*, 7(5):565–73, May 2007.

[49] J. Park, V. Sunkara, T.-H. Kim, H. Hwang, and Y.-K. Cho. Lab-on-a-disc for fully integrated multiplex immunoassays. *Analytical chemistry*, 84(5):2133–40, March 2012.

[50] R. A. Potyrailo, W. G. Morris, A. M. Leach, T. M. Sivavec, M. B. Wisnudel, and S. Boyette. Analog signal acquisition from computer optical disk drives for quantitative chemical sensing. *Analytical chemistry*, 78(16):5893–5899, 2006.

[51] S. K. Arya, B. Lim, and A. R. A. Rahman. Enrichment, detection and clinical significance of circulating tumor cells. *Lab on a Chip*, pages 1995–2027, 2013.

[52] P. Li, Z. S. Stratton, M. Dao, J. Ritz, and T. J. Huang. Probing circulating tumor cells in microfluidics. *Lab on a chip*, 13(4):602–9, March 2013.

[53] E. S. Lianidou and A. Markou. Circulating tumor cells in breast cancer: detection systems, molecular characterization, and future challenges. *Clinical chemistry*, 57(9):1242–55, September 2011.

[54] M. Cristofanilli. Circulating tumor cells, disease progression, and survival in metastatic breast cancer. *Seminars in oncology*, 33(3 Suppl 9):S9–14, June 2006.

[55] H. I. Scher, X. Jia, J. S. de Bono, M. Fleisher, K. J. Pienta, D. Raghavan, and G. Heller. Circulating tumour cells as prognostic markers in progressive, castration-resistant prostate cancer: a reanalysis of IMMC38 trial data. *The lancet oncology*, 10(3):233–9, March 2009.

[56] S. Nagrath, L. V. Sequist, S. Maheswaran, D. W. Bell, D. Irimia, L. Ulkus, M. R. Smith, E. L. Kwak, S. Digumarthy, A. Muzikansky, P. Ryan, U. J. Balis, R. G. Tompkins, D. a. Haber, and M. Toner. Isolation of rare circulating tumour cells in cancer patients by microchip technology. *Nature*, 450(7173):1235–9, December 2007.

[57] J.-M. Park, M. S. Kim, H.-S. Moon, C. E. Yoo, D. Park, Y. J. Kim, K.-Y. Han, J.-Y. Lee, J. H. Oh, S. S. Kim, W.-Y. Park, W.-Y. Lee, and N. Huh. Fully automated circulating tumor cell isolation platform with large-volume capacity based on lab-on-a-disc. *Analytical chemistry*, 86(8):3735–42, April 2014.

[58] S. Mocellin, U. Keilholz, C. R. Rossi, and D. Nitti. Circulating tumor cells: the 'leukemic phase' of solid cancers. *Trends in molecular medicine*, 12(3):130–9, March 2006.

[59] S. L. Stott, C.-H. Hsu, D. I. Tsukrov, M. Yu, D. T. Miyamoto, B. a. Waltman, S. M. Rothenberg, A. M. Shah, M. E. Smas, G. K. Korir, F. P. Floyd, A. J. Gilman, J. B. Lord, D. Winokur, S. Springer, D. Irimia, S. Nagrath, L. V. Sequist, R. J. Lee, K. J. Isselbacher, S. Maheswaran, D. a. Haber, and M. Toner. Isolation of circulating tumor cells using a microvortex-generating herringbone-chip. *Proceedings of the National Academy of Sciences of the United States of America*, 107(43):18392–7, October 2010.

[60] J. Autebert, B. Coudert, F.-C. Bidard, J.-Y. Pierga, S. Descroix, L. Malaquin, and J.-L. Viovy. Microfluidic: an innovative tool for efficient cell sorting. *Methods (San Diego, Calif.)*, 57(3):297–307, July 2012.

[61] J. Chen, J. Li, and Y. Sun. Microfluidic approaches for cancer cell detection, characterization, and separation. *Lab on a chip*, 12(10):1753–67, April 2012.

[62] I. Cima, C. Wen Yee, F. S. Iliescu, W. Min Phyo, K. Hon Lim, C. Iliescu, and M. Han Tan. Label-free isolation of circulating tumor cells in microfluidic devices: Current research and perspectives. *Biomicrofluidics*, 7(1):011810, 2013.

[63] Z. Zhang and S. Nagrath. Microfluidics and cancer: are we there yet? *Biomedical microdevices*, January 2013.

[64] G. Vona, A. Sabile, M. Louha, V. Sitruk, S. Romana, K. Schütze, F. Capron, D. Franco, M. Pazzagli, M. Vekemans, et al. Isolation by size of epithelial tumor cells: a new method for the immunomorphological and molecular characterization of circulating tumor cells. *The American journal of pathology*, 156(1):57–63, 2000.

[65] V. Müller, N. Stahmann, S. Riethdorf, T. Rau, T. Zabel, A. Goetz, F. Jänicke, and K. Pantel. Circulating tumor cells in breast cancer: correlation to bone marrow micrometastases, heterogeneous response to systemic therapy and low proliferative activity. *Clinical Cancer Research*, 11(10):3678–3685, 2005.

[66] D. Di Carlo. Inertial microfluidics. *Lab on a chip*, 9(21):3038–46, November 2009.

[67] A. Ymeti, X. Li, B. Lunter, C. Breukers, A. G. Tibbe, L. W. Terstappen, and J. Greve. A single platform image cytometer for resource-poor settings to monitor disease progression in hiv infection. *Cytometry Part A*, 71(3):132–142, 2007.

[68] K. Hoshino, Y.-Y. Huang, N. Lane, M. Huebschman, J. W. Uhr, E. P. Frenkel, and X. Zhang. Microchip-based immunomagnetic detection of circulating tumor cells. *Lab on a chip*, 11(20):3449–57, October 2011.

[69] D. Issadore, J. Chung, H. Shao, M. Liong, A. A. Ghazani, C. M. Castro, R. Weissleder, and H. Lee. Ultrasensitive clinical enumeration of rare

cells ex vivo using a micro-hall detector. *Science translational medicine*, 4(141):141ra92, July 2012.

[70] J. H. Kang, S. Krause, H. Tobin, A. Mammoto, M. Kanapathipillai, and D. E. Ingber. A combined micromagnetic-microfluidic device for rapid capture and culture of rare circulating tumor cells. *Lab on a chip*, 12(12):2175–81, June 2012.

[71] N. Pamme. On-chip bioanalysis with magnetic particles. *Current opinion in chemical biology*, 16(3-4):436–43, August 2012.

[72] M. Helou, M. Reisbeck, S. F. Tedde, L. Richter, L. Bär, J. J. Bosch, R. H. Stauber, E. Quandt, and O. Hayden. Time-of-flight magnetic flow cytometry in whole blood with integrated sample preparation. *Lab on a chip*, 13(6):1035–8, February 2013.

[73] J. Darabi and C. Guo. On-chip magnetophoretic isolation of CD4+T cells from blood. *Biomicrofluidics*, 7(5):54106, January 2013.

[74] L. Riegger, M. Grumann, J. Steigert, S. Lutz, C. P. Steinert, C. Mueller, J. Viertel, O. Prucker, J. Rühe, R. Zengerle, and J. Ducrée. Single-step centrifugal hematocrit determination on a 10-$ processing device. *Biomedical microdevices*, 9(6):795–9, December 2007.

[75] M. T. Glynn, D. J. Kinahan, and J. Ducrée. CD4 counting technologies for HIV therapy monitoring in resource-poor settings–state-of-the-art and emerging microtechnologies. *Lab on a chip*, 13(14):2731–48, July 2013.

[76] S. C. Hur, A. J. Mach, and D. Di Carlo. High-throughput size-based rare cell enrichment using microscale vortices. *Biomicrofluidics*, 5(2):022206, 2011.

[77] R. Königsberg, E. Obermayr, G. Bises, G. Pfeiler, M. Gneist, F. Wrba, M. de Santis, R. Zeillinger, M. Hudec, and C. Dittrich. Detection of epcam positive and negative circulating tumor cells in metastatic breast cancer patients. *Acta oncologica*, 50(5):700–710, 2011.

[78] M. Glynn, D. Kirby, C. N. D. Kinahan, C. Spillane, O. Shiels, J. OLeary, and J. Ducrée. Staging the clinical status from blood of cancer patients by chip-based cell enumeration following targetted removal of normal cells. *Proceedings of The 18th International Conference on Miniaturized Systems for Chemistry and Life Sciences microTAS 2014*, pages 461–463, 2014.

[79] Y.-F. Sun, X.-R. Yang, J. Zhou, S.-J. Qiu, J. Fan, and Y. Xu. Circulating tumor cells: advances in detection methods, biological issues, and clinical relevance. *Journal of cancer research and clinical oncology*, 137(8):1151–1173, 2011.

[80] L. Liang, J. Zhu, and X. Xuan. Three-dimensional diamagnetic particle deflection in ferrofluid microchannel flows. *Biomicrofluidics*, 5(3):034110, 2011.

[81] C. Grundy, A. Medina Lara, D. Winogron, et al. Point-of-care cd4 tests can increase life-years saved with reduced costs compared to flow cytometric cd4 counting. In *Sixth International AIDS Society Conference on HIV Pathogenesis, Treatment and Prevention*, 2011.

[82] I. V. Jani, N. E. Sitoe, E. R. Alfai, P. L. Chongo, J. I. Quevedo, B. M. Rocha, J. D. Lehe, and T. F. Peter. Effect of point-of-care cd4 cell count tests on retention of patients and rates of antiretroviral therapy initiation in primary health clinics: an observational cohort study. *The Lancet*, 378(9802):1572–1579, 2011.

[83] D. S. Boyle, K. R. Hawkins, M. S. Steele, M. Singhal, and X. Cheng. Emerging technologies for point-of-care cd4 t-lymphocyte counting. *Trends in biotechnology*, 30(1):45–54, 2012.

[84] M. Glynn, D. Kirby, D. Chung, D. J. Kinahan, G. Kijanka, and J. Ducrée. Centrifugo-magnetophoretic Purification of CD4+ Cells from Whole Blood toward Future HIV/AIDS Point-of-Care Applications. *Journal of laboratory automation*, pages 2211068213504759–, September 2013.

[85] W. H. Organization et al. Rapid advice: antiretroviral therapy for hiv infection in adults and adolescents-november 2009. 2009.

[86] M. T. Glynn, D. J. Kinahan, and J. Ducrée. Rapid, low-cost and instrument-free cd4+ cell counting for hiv diagnostics in resource-poor settings. *Lab on a Chip*, 14(15):2844–2851, 2014.

[87] N. J. Panaro, X. J. Lou, P. Fortina, L. J. Kricka, and P. Wilding. Micropillar array chip for integrated white blood cell isolation and pcr. *Biomolecular engineering*, 21(6):157–162, 2005.

[88] D. R. Gossett, W. M. Weaver, A. J. Mach, S. C. Hur, H. T. K. Tse, W. Lee, H. Amini, and D. Di Carlo. Label-free cell separation and

sorting in microfluidic systems. *Analytical and bioanalytical chemistry*, 397(8):3249–3267, 2010.

[89] M. Godin, A. K. Bryan, T. P. Burg, K. Babcock, and S. R. Manalis. Measuring the mass, density, and size of particles and cells using a suspended microchannel resonator. *Applied physics letters*, 91(12):123121, 2007.

[90] J. Nam, H. Huang, H. Lim, C. Lim, and S. Shin. Magnetic separation of malaria-infected red blood cells in various developmental stages. *Analytical chemistry*, 85(15):7316–7323, 2013.